A kinetic model for the sedimentation of rod-like particles

Christian Helzel and Felix Otto and A. E. Tzavaras

A KINETIC MODEL FOR THE SEDIMENTATION OF ROD–LIKE PARTICLES

CHRISTIANE HELZEL*, FELIX OTTO†, AND ATHANASIOS E. TZAVARAS ‡

Abstract. We consider a kinetic multi-scale model, describing suspensions of rod-like particles, which couples a microscopic Smoluchowski equation - for the distribution of rod orientations - to a macroscopic Stokes or Navier-Stokes equation via an elastic stress tensor and a gravitational forcing term. A reciprocal coupling of phenomena on these different scales leads to the formation of clusters. The buoyancy force creates a macroscopic velocity gradient that causes the microscopic particles to align in such a way that their sedimentation reinforces the formation of clusters of higher particle density.

We perform a linear stability analysis and show that linear theory can predict a wavelength selection mechanism for the cluster width, provided that the Reynolds number is larger than zero. An asymptotic analysis of the largest eigenvalue around $Re = 0$ explains this response, while numerical simulations of the nonlinear model confirm the wavelength selection. By looking at special flow configurations and at parameter scalings, we derive simpler models which describe the aggregate behavior of the suspension in various regimes. In particular, in a diffusive type of scaling, we obtain the two-dimensional Keller-Segel model.

Key words. sedimentation, rod-like particles, linear stability, asymptotic expansions

AMS subject classifications. 76T20, 74A25, 35B40

1. Introduction. Complex fluids are fluids with a suspended microstructure such as polymers with a long chain structure. A simplified model is that of suspensions of rod-like particles. In such systems multiscale interactions can cause interesting phenomena. The macroscopic flow leads to a change of the orientation and shape (in the case of flexible particles) of the suspended microstructure. In turn, this produces a fluid stress which interacts with and modifies the macroscopic flow.

Here we consider the sedimentation of dilute suspensions of rod-like particles under gravity. This problem exhibits interesting pattern formations and has been studied by several authors in theoretical, numerical and experimental work. Understanding sedimentation is of importance in recycling processes of the paper industry [7], and related models arise also in the description of self-locomotion [20]. In contrast to spherical particles, rod-like particles have an orientation, what adds complexity to the sedimentation process. For instance, the sedimentation velocity of a single particle depends on its orientation. Furthermore, a particle falls not only in the gravity direction but also sidewards. By restricting considerations to rigid rods we eliminate deformation effects such as bending of polymers. While previous experimental and numerical work studies the sedimentation of non-Brownian particles, we mainly concentrate on the case of Brownian particles.

The kinetic model considered here is an extension of the Doi model for dilute suspensions of rod-like particles described in Doi and Edwards [5]. In previous work we considered the Doi model for suspensions of rod-like molecules neglecting the effects of gravity, see [9], [16].

The sedimentation of fibers has been studied in experimental work for instance by Guazzelli and coworkers [10, 11, 14]. These experiments reveal the following scenarios: Starting from a well-stirred suspension packets of particles form after some time. These packets seem to have a mesoscopic equilibrium width, suggesting that the density of particles acquires variations of a characteristic length scale. Within such a cluster, individual particles are aligned with the direction of gravity during most of the time; occasionally they flip. The average settling speed in a suspension is larger than the sedimentation speed of a single particle oriented in the direction of gravity.

In recent years the sedimentation of rod-like particles (and other orientable particles) has also been studied via numerical simulations of multi-scale models. Gustavsson and Tornberg [8, 21] used a very detailed description of rod-like particles in a dilute suspension based on a slender body approximation. They were able to simulate suspensions with up to a few hundred particles and a domain size of the order of a few particle length. Butler and Shaqfeh [2] used a lower order slender body description. Saintillan et al. [17] accelerated this algorithm using fast summation techniques. This allowed them to

*Department of Mathematics, Ruhr-University Bochum, Germany christiane.helzel@rub.de,

†Institute of Applied Mathematics, University of Bonn, Germany otto@iam.uni-bonn.de

‡Department of Applied Mathematics, University of Crete, Heraklion, Greece
and Institute for Applied and Computational Mathematics , FORTH, Heraklion, Greece, tzavaras@tem.uoc.gr

simulate several thousand particles. Wang and Layton [22] used the immersed boundary method for their two-dimensional numerical studies. All numerical results confirm the basic experimental findings: Packet formation and alignment in gravity direction (at least for higher concentration). Note that the models used in these simulations are of more microscopic nature than the model considered here. Instead of a number density function for the rod orientation in every point of the domain, those authors consider a large number of individual particles. Moreover, Brownian effects are not considered, which amounts to setting the absolute temperature $\theta = 0$ in our model.

Koch and Shaqfeh [12] performed a linear stability analysis for a related kinetic model by neglecting Brownian effects. They found a purely imaginary continuum spectrum, but also a point spectrum with positive real part. This predicts instability of density modulations for horizontal waves with a sufficiently small wavenumber but not a wavelength selection mechanism. The introduction of Brownian effects in terms of translational diffusion does also not provide a wavelength selection mechanism at the level of linear stability analysis, see Saintillan et al. [19].

In the case of non-Brownian sedimentation of spherical particles, there is a mathematically related divergence of fluctuations at long wavelength [3]. For that physical system, a small stable density stratification has been proposed as a mechanism which suppresses this long wavelength divergence [13]. In the case of sedimenting rod-like particles it also leads to a wavelength selection at the level of linear stability analysis [18]. In experiments and numerical simulations, this stratification may be induced by the boundary conditions at the horizontal container walls [18]. However, the predicted scaling of the unstable wavelength does not agree with experiments [15].

Our objective in this work is on one hand to address the issue of initial wavelength selection, and on the other to discuss the subsequent mechanism of aggregation. We employ a kinetic model in the spirit of Doi theory focusing on dilute suspensions of rod-like particles. We first present an analysis of the thermodynamic consistency of the kinetic model and pursue a non-dimensional analysis. There are three non-dimensional parameters in the problem. The Reynolds number which quantifies the relative importance of inertial forces versus viscous forces and two additional non-dimensional parameters which measure the importance of the rate of work due to elastic force vs. buoyancy as well as buoyancy vs. viscous force. The influence of these parameters on linear stability theory is studied. In Section 3 we present a linear stability analysis which includes also the effects of rotational diffusion. We show: If the macroscopic flow is modeled by the Stokes equation, linear stability theory does not predict a wavelength selection mechanism. However, if the macroscopic flow is modeled by the Navier-Stokes equation (i.e. $Re > 0$), we obtain a wavelength selection mechanism. This behavior is explained by doing a (singular) perturbation analysis of the largest eigenvalue in Reynolds number.

In Section 4, we perform the stability analysis for the sedimentation of non-Brownian particles. While we do not have a theoretical justification for the use of the linear model in the case of non-Brownian particles, we show that the predictions of the linear model are in good agreement with numerical simulations of the nonlinear model.

Finally, in Section 5 we derive the aggregate behavior of the suspension in various parameter scalings. We show that for a particular flow configuration and a diffusive scaling of the equations the density follows a nonlinear concentration mechanism that is captured by the well-known two-dimensional Keller-Segel model. Related derivations of macroscopic models as limits of kinetic models can be found in [4, 6]

We also present numerical simulations for the coupled nonlinear multi-scale model which indicate the initial wavelength selection as well as capture the subsequent concentration.

2. The mathematical model. We describe a kinetic model for sedimentation in dilute suspensions of rod-like Brownian particles. Models of this type were introduced by Doi and Edwards, see [5, Ch. 8]. In [16] a related model for suspensions of rod-like particles was considered. Here we extend this model to account for the effects of gravity.

We consider inflexible rod-like particles of thickness b which is much smaller than the particles length l. Our considerations are restricted to the dilute regime which is characterized by the relation $\nu \ll l^{-3}$ where ν is the number density. Note that in contrast to the model considered in [16], the number density is not constant here. The orientation of a rod-like particle is characterized by $\boldsymbol{n} \in S^{d-1}$ where d is the dimension of the macroscopic physical space $\Omega \subset \mathbb{R}^d$.

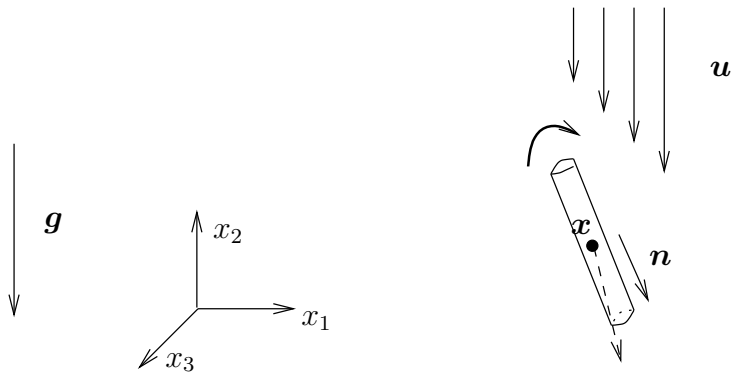

FIG. 2.1. *Basic notation for rod-like molecule which is falling sidewards.*

We denote by $\boldsymbol{e}_2$ the unit vector in the upward direction and by $\boldsymbol{g} = -g\boldsymbol{e}_2$ the acceleration of gravity with gravitational constant g. Furthermore, let m_0 denote the mass of an individual rod-like particle and $\boldsymbol{G} = -m_0 g\boldsymbol{e}_2$ be the force of gravity on a single particle. Some of our basic notation is depicted in Figure 2.1.

In a quiescent suspension (i.e. macroscopic velocity $\boldsymbol{u} = 0$) each particle sediments at a speed depending on its orientation $\boldsymbol{n}$ according to

$$\begin{aligned}\frac{d\boldsymbol{x}}{dt} &= \frac{1}{\zeta_{||}}\left(\boldsymbol{G}\cdot\boldsymbol{n}\right)\boldsymbol{n} + \frac{1}{\zeta_{\perp}}\left(\boldsymbol{G} - \left(\boldsymbol{G}\cdot\boldsymbol{n}\right)\boldsymbol{n}\right)\\ &= \left(\frac{1}{\zeta_{||}}\boldsymbol{n}\otimes\boldsymbol{n} + \frac{1}{\zeta_{\perp}}\left(I - \boldsymbol{n}\otimes\boldsymbol{n}\right)\right)\boldsymbol{G}\\ &= \frac{1}{\zeta_{\perp}}\left(\boldsymbol{n}\otimes\boldsymbol{n} + I\right)\boldsymbol{G}\end{aligned}$$

where $\zeta_{||}$ and $\zeta_{\perp}$ are the frictional coefficients in the tangential and the normal direction which satisfy $\zeta_{\perp} = 2\zeta_{||}$. In particular, a particle with a horizontal orientation sediments slower than a particle with a vertical orientation and a particle of oblique orientation moves also sideways.

In addition a macroscopic velocity gradient causes a rotation according to the equation

$$\frac{d\boldsymbol{n}}{dt} = P_{\boldsymbol{n}^{\perp}}\nabla_{\boldsymbol{x}}\boldsymbol{u}\boldsymbol{n}$$

where $P_{\boldsymbol{n}^{\perp}}\nabla_{\boldsymbol{x}}\boldsymbol{u}\boldsymbol{n} := \nabla_{\boldsymbol{x}}\boldsymbol{u}\boldsymbol{n} - \left(\nabla_{\boldsymbol{x}}\boldsymbol{u}\boldsymbol{n}\cdot\boldsymbol{n}\right)\boldsymbol{n}$ is the projection of the vector $\nabla_{\boldsymbol{x}}\boldsymbol{u}\boldsymbol{n}$ on the tangent space at $\boldsymbol{n}$.

We next include the effects of rotational and translational Brownian motion and account for the macroscopic mean flow $\boldsymbol{u}(\boldsymbol{x}, t)$. The model then becomes the system of stochastic differential equations

$$\begin{aligned}d\boldsymbol{x} &= \boldsymbol{u}dt + \left(\frac{1}{\zeta_{||}}\boldsymbol{n}\otimes\boldsymbol{n} + \frac{1}{\zeta_{\perp}}\left(I - \boldsymbol{n}\otimes\boldsymbol{n}\right)\right)\boldsymbol{G}\,dt\\ &\quad + \sqrt{\frac{2k_B\theta}{\zeta_{||}}\boldsymbol{n}\otimes\boldsymbol{n} + \frac{2k_B\theta}{\zeta_{\perp}}\left(I - \boldsymbol{n}\otimes\boldsymbol{n}\right)}\,dW\\ d\boldsymbol{n} &= P_{\boldsymbol{n}^{\perp}}\nabla_{\boldsymbol{x}}\boldsymbol{u}\boldsymbol{n}\,dt + \sqrt{\frac{2k_B\theta}{\zeta_r}}\,dB\end{aligned} \tag{2.1}$$

where W is the translational Brownian motion and B is the rotational Brownian motion, ζ_r is the rotational friction coefficient, k_B is the Boltzmann constant and θ the absolute temperature .

The above stochastic equations may be equivalently expressed via the Smoluchowski equation for

the evolution of the *local orientational distribution function*:

$$\begin{aligned}\partial_t f + \nabla_{\boldsymbol{x}} \cdot \left[\left(\boldsymbol{u} + \frac{1}{\zeta_\perp} \left(\boldsymbol{n} \otimes \boldsymbol{n} + I \right) \left(-m_0 g \boldsymbol{e}_2 \right) \right) f \right] + \nabla_{\boldsymbol{n}} \cdot \left(P_{\boldsymbol{n}^\perp} \nabla_{\boldsymbol{x}} \boldsymbol{u} \boldsymbol{n} f \right) \\ = \frac{k_B \theta}{\zeta_r} \Delta_{\boldsymbol{n}} f + \frac{k_B \theta}{\zeta_\perp} \nabla_{\boldsymbol{x}} \cdot \left(\boldsymbol{n} \otimes \boldsymbol{n} + I \right) \nabla_{\boldsymbol{x}} f.\end{aligned} \tag{2.2}$$

Here $f(\boldsymbol{x}, t, \boldsymbol{n})\, d\boldsymbol{n}$ describes the number of particles per unit volume at macroscopic position $\boldsymbol{x}$ and time t with orientations in the element centered at $\boldsymbol{n}$ and of volume $d\boldsymbol{n}$. The second term on the left hand side of (2.2) models transport of the center of mass of the particles due to the macroscopic flow velocity and due to gravity. The last term on the left hand side models the rotation of the axis due to a macroscopic velocity gradient $\nabla_{\boldsymbol{x}} \boldsymbol{u}$. The terms on the right hand side describe rotational as well as translational diffusion. The gradient, divergence and Laplacian on the sphere are denoted by $\nabla_{\boldsymbol{n}}$, $\nabla_{\boldsymbol{n}} \cdot$ and $\Delta_{\boldsymbol{n}}$, while the gradient and divergence in the macroscopic flow domain are denoted by $\nabla_{\boldsymbol{x}}$ and $\nabla_{\boldsymbol{x}} \cdot$. The total number of rod-like particles is

$$\int_\Omega \int_{S^{d-1}} f(\boldsymbol{x}, t, \boldsymbol{n})\, d\boldsymbol{n}\, d\boldsymbol{x} = \int_\Omega \int_{S^{d-1}} f(\boldsymbol{x}, 0, \boldsymbol{n})\, d\boldsymbol{n}\, d\boldsymbol{x} = N,$$

i.e. f has dimensions of number density. It is convenient to rewrite the Smoluchowski equation in the form

$$\begin{aligned}\partial_t f + \nabla_{\boldsymbol{x}} \cdot (\boldsymbol{u} f) + \nabla_{\boldsymbol{n}} \cdot \left(P_{\boldsymbol{n}^\perp} \nabla_{\boldsymbol{x}} \boldsymbol{u} \boldsymbol{n} f \right) \\ = D_r \Delta_{\boldsymbol{n}} f + D_\perp \nabla_{\boldsymbol{x}} \cdot \left(I + \boldsymbol{n} \otimes \boldsymbol{n} \right) \left(\nabla_{\boldsymbol{x}} f + \frac{1}{k_B \theta} f \nabla_{\boldsymbol{x}} U \right),\end{aligned} \tag{2.3}$$

where $D_r := \frac{k_B \theta}{\zeta_r}$ and $D_\perp := \frac{k_B \theta}{\zeta_\perp}$ stand for the rotational and translational diffusion coefficients and $U(x) = m_0 g(\boldsymbol{x} \cdot \boldsymbol{e}_2)$ is the potential of the gravity force $\boldsymbol{G} = -\nabla U = -m_0 g \boldsymbol{e}_2$.

As can be seen from (2.3), a velocity gradient $\nabla_{\boldsymbol{x}} \boldsymbol{u}$ distorts an isotropic distribution f which leads to an increase in entropy. Thermodynamic consistency requires (compare with Section 2.1), that this is balanced by a stress tensor $\sigma(\boldsymbol{x}, t)$ given by

$$\sigma(\boldsymbol{x}, t) := k_B \theta \int_{S^{d-1}} \left(d\boldsymbol{n} \otimes \boldsymbol{n} - I \right) f(\boldsymbol{x}, t, \boldsymbol{n}) d\boldsymbol{n}. \tag{2.4}$$

Local variations in the density $m_0 \int_{S^{d-1}} f d\boldsymbol{n}$ lead to spatial variations of the specific weight of the suspension that generally can not be compensated by a hydrostatic pressure and thus trigger a fluid motion (buoyancy). The macroscopic flow is described by the Navier-Stokes equation. Let ρ_f be the density of the fluid which is assumed to be constant. The balance laws of mass and momentum have the form

$$\begin{aligned}\rho_f \left(\partial_t \boldsymbol{u} + \left(\boldsymbol{u} \cdot \nabla_{\boldsymbol{x}} \right) \boldsymbol{u} \right) = \mu \triangle_{\boldsymbol{x}} \boldsymbol{u} - \nabla_{\boldsymbol{x}} p + \nabla_{\boldsymbol{x}} \cdot \sigma \\ - \rho_f g \boldsymbol{e}_2 - \Big(\int_{S^{d-1}} f d\boldsymbol{n} \Big) m_0 g \boldsymbol{e}_2 \\ \nabla_{\boldsymbol{x}} \cdot \boldsymbol{u} = 0\end{aligned} \tag{2.5}$$

The term $\rho_f g \boldsymbol{e}_2$ can be incorporated to the pressure. For the linear stability analysis it will be convenient to express the momentum equation in the equivalent form

$$\begin{aligned}\rho_f \left(\partial_t \boldsymbol{u} + \left(\boldsymbol{u} \cdot \nabla_{\boldsymbol{x}} \right) \boldsymbol{u} \right) = \mu \Delta_{\boldsymbol{x}} \boldsymbol{u} - \nabla_{\boldsymbol{x}} p' + \nabla_{\boldsymbol{x}} \cdot \sigma + \left(\frac{N}{V} - \int_{S^{d-1}} f\, d\boldsymbol{n} \right) m_0 g \boldsymbol{e}_2 \\ \nabla_{\boldsymbol{x}} \cdot \boldsymbol{u} = 0\end{aligned} \tag{2.6}$$

by redefining the pressure,

$$p' = p + \rho_f g \boldsymbol{e}_2 \cdot \boldsymbol{x} + \frac{m_0 N g}{V} \boldsymbol{e}_2 \cdot \boldsymbol{x}\,,$$

to account for the hydrostatic pressures, where V is the volume occupied by the suspension and N the total number of rod-like particles.

We summarize the final model :

$$\begin{aligned}\partial_t f &= -\nabla_{\boldsymbol{x}}\cdot(\boldsymbol{u}f) - \nabla_{\boldsymbol{n}}\cdot(P_{\boldsymbol{n}^\perp}\nabla_{\boldsymbol{x}}\boldsymbol{u}\boldsymbol{n}f) + D_r\Delta_{\boldsymbol{n}}f \\ &\quad + D_\perp\nabla_{\boldsymbol{x}}\cdot(I+\boldsymbol{n}\otimes\boldsymbol{n})\left(\nabla_{\boldsymbol{x}}f + \frac{1}{k_B\theta}m_0g\boldsymbol{e}_2 f\right) \qquad (2.7)\\ \sigma(\boldsymbol{x},t) &= k_B\theta\int_{S^{d-1}}(d\boldsymbol{n}\otimes\boldsymbol{n}-I)\,f(\boldsymbol{x},t,\boldsymbol{n})d\boldsymbol{n} \qquad (2.8)\\ \nabla_{\boldsymbol{x}}\cdot\boldsymbol{u} &= 0 \qquad (2.9)\\ \rho_f\left(\partial_t\boldsymbol{u} + (\boldsymbol{u}\cdot\nabla_{\boldsymbol{x}})\,\boldsymbol{u}\right) &= \mu\Delta_{\boldsymbol{x}}\boldsymbol{u} - \nabla_{\boldsymbol{x}}p + \nabla_{\boldsymbol{x}}\cdot\sigma - \Big(\int_{S^{d-1}} f\,d\boldsymbol{n}\Big)m_0g\boldsymbol{e}_2 \qquad (2.10)\end{aligned}$$

2.1. Thermodynamic consistency of the model. To show thermodynamic consistency of the model we use the free energy functional

$$A[f] := \int_\Omega\int_{S^2}(k_B\theta f\ln f + fU(\boldsymbol{x}))\,d\boldsymbol{n}d\boldsymbol{x}, \qquad (2.11)$$

where $U(\boldsymbol{x}) = m_0g\boldsymbol{x}\boldsymbol{e}_2$ is the gravitational potential.

PROPOSITION 2.1. *For f satisfying the Smoluchowski equation* (2.7)*, the free energy $A[f]$ defined in (2.11) satisfies the identity*

$$\begin{aligned}&\partial_t A[f] + D_r k_B\theta\int_\Omega\int_{S^2} f|\nabla_{\boldsymbol{n}}\ln f|^2 d\boldsymbol{n}d\boldsymbol{x}\\ &+ D_\perp k_B\theta\int_\Omega\int_{S^2}\nabla_{\boldsymbol{x}}\big(\ln f + \frac{1}{k_B\theta}U\big)\cdot\big(I+\boldsymbol{n}\otimes\boldsymbol{n}\big)\nabla_{\boldsymbol{x}}\big(\ln f + \frac{1}{k_B\theta}U\big)d\boldsymbol{n}d\boldsymbol{x} \qquad (2.12)\\ &= \int_\Omega\nabla_{\boldsymbol{x}}\boldsymbol{u} : \sigma d\boldsymbol{x} + \int_\Omega m_0g\boldsymbol{e}_2\left(\int_{S^2} f d\boldsymbol{n}\right)\cdot\boldsymbol{u}d\boldsymbol{x}\end{aligned}$$

Moreover, the total energy

$$E[\boldsymbol{u},f] = \int_\Omega\left(\frac{1}{2}\rho_f|\boldsymbol{u}|^2 + \int_{S^2}\Big((k_B\theta)f\ln f + fU(\boldsymbol{x})\Big)d\boldsymbol{n}\right)d\boldsymbol{x} \qquad (2.13)$$

of the system (2.7)-(2.10) *dissipates.*

Proof: We differentiate (2.11) with respect to t,

$$\partial_t A[f] = \int_\Omega\int_{S^2}\Big(k_B\theta(1+\ln f) + U(\boldsymbol{x})\Big)f_t\,d\boldsymbol{n}d\boldsymbol{x} \qquad (2.14)$$

and use (2.7) to express the various contributions.

The contribution of the transport term $-\nabla_{\boldsymbol{x}}\cdot(\boldsymbol{u}f)$ gives

$$\begin{aligned}I_{tr} &= -\int_\Omega\int_{S^2}\Big(k_B\theta(1+\ln f) + U(\boldsymbol{x})\Big)\nabla_{\boldsymbol{x}}\cdot(\boldsymbol{u}f)\,d\boldsymbol{n}d\boldsymbol{x}\\ &= \int_\Omega\int_{S^2}\Big(k_B\theta\nabla_{\boldsymbol{x}}f + f\nabla_{\boldsymbol{x}}U\Big)\cdot\boldsymbol{u}d\boldsymbol{n}d\boldsymbol{x}\\ &\overset{(2.9)}{=} \int_\Omega m_0g\boldsymbol{e}_2\left(\int_{S^2} f d\boldsymbol{n}\right)\cdot\boldsymbol{u}\,d\boldsymbol{x}\end{aligned}$$

Next, consider the contribution of the drift term $-\nabla_{\boldsymbol{n}} \cdot (P_{\boldsymbol{n}^\perp} \nabla_{\boldsymbol{x}} \boldsymbol{u} \boldsymbol{n} f)$. We obtain:

$$\begin{aligned} I_{dr} &= -\int_\Omega \int_{S^2} \Big(k_B\theta(1+\ln f) + U(\boldsymbol{x})\Big) \nabla_{\boldsymbol{n}} \cdot (P_{\boldsymbol{n}^\perp} \nabla_{\boldsymbol{x}} \boldsymbol{u} \boldsymbol{n} f)\, d\boldsymbol{n} d\boldsymbol{x} \\ &\overset{(B.1)}{=} \int_\Omega \int_{S^2} k_B\theta \nabla_{\boldsymbol{n}} \ln f \cdot P_{\boldsymbol{n}^\perp} (\nabla_{\boldsymbol{x}} \boldsymbol{u} \boldsymbol{n} f)\, d\boldsymbol{n} d\boldsymbol{x} \\ &= \int_\Omega \nabla_{\boldsymbol{x}} \boldsymbol{u} : k_B\theta \int_{S^2} \boldsymbol{n} \otimes \nabla_{\boldsymbol{n}} f \, d\boldsymbol{n}\, d\boldsymbol{x} \\ &\overset{(B.3),(2.8)}{=} \int_\Omega \nabla_{\boldsymbol{x}} \boldsymbol{u} : \sigma \, d\boldsymbol{x}. \end{aligned}$$

The contribution of rotational diffusion is:

$$\begin{aligned} I_{rd} &= \int_\Omega \int_{S^2} \Big(k_B\theta(1+\ln f) + U(\boldsymbol{x})\Big) D_r \Delta_{\boldsymbol{n}} f \, d\boldsymbol{n} d\boldsymbol{x} \\ &= \int_\Omega \int_{S^2} \Big(k_B\theta(1+\ln f) + U(\boldsymbol{x})\Big) D_r \nabla_{\boldsymbol{n}} \cdot (f \nabla_{\boldsymbol{n}} \ln f)\, d\boldsymbol{n} d\boldsymbol{x} \\ &= -\frac{(k_B\theta)^2}{\zeta_r} \int_\Omega \int_{S^2} |\nabla_{\boldsymbol{n}} \ln f|^2 f \, d\boldsymbol{n} d\boldsymbol{x} \end{aligned}$$

Finally, the contribution of the last term in (2.7), modeling translational friction and translational diffusion, reads

$$\begin{aligned} I_{tdf} &= \int_\Omega \int_{S^2} \Big(k_B\theta(1+\ln f) + U(\boldsymbol{x})\Big) D_\perp \nabla_{\boldsymbol{x}} \cdot (I + \boldsymbol{n} \otimes \boldsymbol{n}) \left(\nabla_{\boldsymbol{x}} f + \frac{f}{k_B\theta} \nabla_{\boldsymbol{x}} U\right) \\ &= -\frac{(k_B\theta)^2}{\zeta_\perp} \int_{S^2} \int_\Omega \nabla_{\boldsymbol{x}} \left(\ln f + \frac{1}{k_B\theta} U\right) \cdot (I + \boldsymbol{n} \otimes \boldsymbol{n}) f \nabla_{\boldsymbol{x}} \left(\ln f + \frac{1}{k_B\theta} U\right) \end{aligned}$$

Combining all these contributions together yields (2.12).

Next, we multiply the Navier-Stokes equation (2.10) by $\boldsymbol{u}$ and integrate over Ω to obtain the balance of the kinetic energy

$$\begin{aligned} \frac{d}{dt} \int_\Omega \frac{1}{2} \rho_f |\boldsymbol{u}|^2 d\boldsymbol{x} + \mu \int_\Omega \nabla_{\boldsymbol{x}} \boldsymbol{u} : \nabla_{\boldsymbol{x}} \boldsymbol{u} \, d\boldsymbol{x} \\ = -\int_\Omega \nabla_{\boldsymbol{x}} \boldsymbol{u} : \sigma \, d\boldsymbol{x} - \int_\Omega \boldsymbol{u} \cdot m_0 g \boldsymbol{e}_2 \left(\int_{S^2} f d\boldsymbol{n}\right) d\boldsymbol{x}\,. \end{aligned} \tag{2.15}$$

Combining (2.12) and (2.15) leads to the balance of total energy. In particular, it follows that the total energy dissipates.

2.2. Non-dimensionalization. We first list the dimensions of the terms that appear in the equations. The units of mass, length and time are denoted by M, L and T. We also monitor the dependence on the number of particles N.

- v: velocity $\left[\frac{L}{T}\right]$
- $m_0 g$: mass $\times$ acceleration $\left[\frac{ML}{T^2}\right]$;
- $k_B\theta$: energy = force $\times$ length $\left[\frac{ML^2}{T^2}\right]$
- $\zeta_\perp$: translational friction orthogonal to rod = force / velocity $\left[\frac{M}{T}\right]$
  $D_\perp = \frac{k_B\theta}{\zeta_\perp}$ $\left[\frac{L^2}{T}\right]$
- ζ_r: rotational friction = torque / rotatational velocity $\left[\frac{ML^2}{T}\right]$
  $D_r = \frac{k_B\theta}{\zeta_r}$ $\left[\frac{1}{T}\right]$
- $\mu = \dfrac{\text{force/area}}{\text{velocity gradient}}$ $\left[\frac{M}{LT}\right]$
- p: pressure = force/area $\left[\frac{M}{LT^2}\right]$

- f: number of particles / volume $\left[\frac{N}{L^3}\right]$
- $\sigma \sim (k_B\theta) f$ $\left[\frac{MN}{LT^2}\right]$

Now we consider a change of scale of the form

$$t = T\hat{t},\ \boldsymbol{x} = X\hat{\boldsymbol{x}},\ \boldsymbol{u} = \frac{X}{T}\hat{\boldsymbol{u}},\ f = \frac{N}{V}\hat{f},\ p = \frac{\mu}{T}\hat{p},\ \sigma = (k_B\theta)\frac{N}{V}\hat{\sigma}. \tag{2.16}$$

We have used two length scales in (2.16): a length scale X that will be selected in the course of the non-dimensionalization process, and a length scale L standing for the size of the macroscopic domain and entering only through the volume occupied by the suspension $V = O(L^3)$.

In these new units the Smoluchowski equation takes the form

$$\begin{aligned} &\partial_{\hat{t}}\hat{f} + \nabla_{\hat{\boldsymbol{x}}}\cdot\left(\hat{\boldsymbol{u}}\hat{f}\right) + \nabla_{\boldsymbol{n}}\cdot\left(P_{\boldsymbol{n}^\perp}\nabla_{\hat{\boldsymbol{x}}}\hat{\boldsymbol{u}}\boldsymbol{n}\hat{f}\right) = TD_r\Delta_{\boldsymbol{n}}\hat{f} \\ &+ \frac{T}{X^2}D_\perp\nabla_{\hat{\boldsymbol{x}}}\cdot\left(I+\boldsymbol{n}\otimes\boldsymbol{n}\right)\nabla_{\hat{\boldsymbol{x}}}\hat{f} + \frac{D_\perp}{X}T\frac{m_0 g}{k_B\theta}\nabla_{\hat{\boldsymbol{x}}}\cdot\left(\left(I+\boldsymbol{n}\otimes\boldsymbol{n}\right)\boldsymbol{e}_2\hat{f}\right) \end{aligned} \tag{2.17}$$

We select the time scale T to be the time scale of the rotational Brownian motion, i.e. we set

$$T = \frac{1}{D_r}. \tag{2.18}$$

Furthermore, we select the length scale X via

$$X = \frac{m_0 g}{\zeta_\perp D_r}. \tag{2.19}$$

This selection corresponds to a velocity scale

$$\frac{X}{T} = \frac{m_0 g}{\zeta_\perp}, \tag{2.20}$$

i.e. the velocity scale is proportional to the motion of a single rod falling due to gravity in a friction dominated flow.

Using (2.18)-(2.20) in Equation (2.17) we obtain the kinetic equation in the dimensionless form

$$\begin{aligned} \partial_{\hat{t}}f + \nabla_{\hat{\boldsymbol{x}}}\cdot\left(\hat{\boldsymbol{u}}f\right) + \nabla_{\hat{\boldsymbol{n}}}\cdot\left(P_{\boldsymbol{n}^\perp}\nabla_{\boldsymbol{x}}\hat{\boldsymbol{u}}\boldsymbol{n}f\right)\boldsymbol{e}_2 f - \nabla_{\hat{\boldsymbol{x}}}\cdot\left(\left(I+\boldsymbol{n}\otimes\boldsymbol{n}\right)\boldsymbol{e}_2 f\right) \\ = \Delta_{\boldsymbol{n}}f + \gamma\nabla_{\hat{\boldsymbol{x}}}\cdot\left(I+\boldsymbol{n}\otimes\boldsymbol{n}\right)\nabla_{\hat{\boldsymbol{x}}}f, \end{aligned} \tag{2.21}$$

with the dimensionless parameter

$$\gamma := \frac{k_B\theta\zeta_\perp D_r}{(m_0 g)^2}. \tag{2.22}$$

Remark 2.1. *The parameter γ measures the relation of the work of elastic forces vs. the work of buoyancy.*

Recall the equation (2.15) for the rate of change of the kinetic energy of the fluid

$$\begin{aligned} &\partial_t\int \rho_f\frac{1}{2}|\boldsymbol{u}|^2 d\boldsymbol{x} \\ &= -\underbrace{\int \mu\nabla_{\boldsymbol{x}}\boldsymbol{u} : \nabla_{\boldsymbol{x}}\boldsymbol{u} d\boldsymbol{x}}_{\text{rate of energy dissipation}} - \underbrace{\int\left(\nabla\boldsymbol{u} : \sigma + \left(\int f d\boldsymbol{n}\right) m_0 g\boldsymbol{u}\cdot\boldsymbol{e}_2\right) d\boldsymbol{x}}_{\text{rate of work of microscopic forces}}. \end{aligned} \tag{2.23}$$

The rate of work of microscopic forces is the sum of the rate of work of elastic forces and the rate of work of buoyancy. Thus we obtain:

$$\begin{aligned} \frac{\text{rate of work of elastic forces}}{\text{rate of work of buoyancy}} &= \left|\frac{\nabla_{\boldsymbol{x}}\boldsymbol{u} : \sigma}{\left(\int f d\boldsymbol{n}\right) m_0 g\boldsymbol{u}\cdot\boldsymbol{e}_2}\right| \\ &\sim \frac{\frac{1}{T}(k_B\theta)|f|}{\frac{X}{T}m_0 g|f|} = \frac{k_B\theta\zeta_\perp D_r}{(m_0 g)^2} = \gamma \end{aligned}$$

The non-dimensionalization of the elastic stress tensor leads to the expression

$$\hat{\sigma} = \int_{S^{d-1}} (d\boldsymbol{n} \otimes \boldsymbol{n} - I)\, \hat{f} d\boldsymbol{n}. \tag{2.24}$$

Finally, we non-dimensionalize the Navier-Stokes equation. We obtain

$$\begin{aligned}&\frac{X^2}{T\mu}\rho_f \left(\partial_{\hat{t}}\hat{\boldsymbol{u}} + (\hat{\boldsymbol{u}} \cdot \nabla_{\hat{\boldsymbol{x}}})\, \hat{\boldsymbol{u}}\right)\\ &= \Delta_{\hat{\boldsymbol{x}}}\hat{\boldsymbol{u}} - \nabla_{\hat{\boldsymbol{x}}}\hat{p} + \frac{XT}{\mu}\frac{k_B\theta}{X}\frac{N}{V}\nabla_{\hat{\boldsymbol{x}}} \cdot \hat{\sigma} - \frac{N}{V}m_0 g\frac{XT}{\mu}\left(\int_{S^{d-1}} \hat{f}\, d\boldsymbol{n}\right)\boldsymbol{e}_2.\end{aligned}$$

There are three non-dimensional numbers emerging: First, a Reynolds number based on the microscopic velocity X/T and the microscopic length scale X,

$$Re := \rho_f \frac{X^2}{T\mu} = \frac{\rho_f}{\mu}\left(\frac{m_0 g}{\zeta_\perp}\right)^2 \frac{1}{D_r}.$$

Second the non-dimensional parameter

$$\delta := \frac{N}{V} m_0 g \frac{XT}{\mu}$$

which is proportional to the number density $\nu = \frac{N}{V}$ and turns out to describe the ratio between buoyancy and viscous forces. The third non-dimensional quantity is a composite, expressed in the form

$$\frac{XT}{\mu}\frac{k_B\theta}{X}\frac{N}{V} = \left(\frac{N}{V}m_0 g\frac{XT}{\mu}\right)\frac{k_B\theta}{m_0 g X} = \delta\frac{k_B\theta\zeta_\perp D_r}{(m_0 g)^2} = \delta\gamma$$

The non-dimensional form of the Navier-Stokes equation is

$$Re\left(\partial_{\hat{t}}\hat{\boldsymbol{u}} + (\hat{\boldsymbol{u}} \cdot \nabla_{\hat{\boldsymbol{x}}})\, \hat{\boldsymbol{u}}\right) = \Delta_{\hat{\boldsymbol{x}}}\hat{\boldsymbol{u}} - \nabla_{\hat{\boldsymbol{x}}}\hat{p} + \delta\gamma\nabla_{\hat{\boldsymbol{x}}} \cdot \sigma - \delta\left(\int_{S^{d-1}} \hat{f}\, d\boldsymbol{n}\right)\boldsymbol{e}_2. \tag{2.25}$$

Remark 2.2. *The parameter δ measures the relation between the rate of work of buoyancy vs. the rate of work of viscous force.*

From (2.23) we express

$$\begin{aligned}\frac{\text{rate of work of buoyancy}}{\text{rate of work of viscous force}} &= \left|\frac{\left(\int f d\boldsymbol{n}\right) m_0 g \boldsymbol{u}\boldsymbol{e}_2}{\mu\left|\nabla\boldsymbol{u}\right|^2}\right|\\ &\sim \frac{\frac{N}{V}m_0 g\frac{X}{T}}{\mu\frac{1}{T^2}} = \frac{N}{V}m_0 g\frac{XT}{\mu} = \delta.\end{aligned} \tag{2.26}$$

We summarize the non-dimensional form of the equations (dropping the hats)

$$\begin{aligned}\partial_t f + \nabla_{\boldsymbol{x}} \cdot (\boldsymbol{u} f) + \nabla_{\boldsymbol{n}} \cdot (P_{\boldsymbol{n}^\perp}\nabla_{\boldsymbol{x}}\boldsymbol{u}\boldsymbol{n} f) - \nabla_{\boldsymbol{x}} \cdot ((I + \boldsymbol{n}\otimes\boldsymbol{n})\,\boldsymbol{e}_2 f)&\\ = \Delta_{\boldsymbol{n}} f + \gamma\nabla_{\boldsymbol{x}} \cdot (I + \boldsymbol{n}\otimes\boldsymbol{n})\,\nabla_{\boldsymbol{x}} f&\\ \sigma = \int_{S^{d-1}} (d\boldsymbol{n}\otimes\boldsymbol{n} - I)\, f\, d\boldsymbol{n}&\\ Re\left(\partial_t\boldsymbol{u} + (\boldsymbol{u}\cdot\nabla_{\boldsymbol{x}})\,\boldsymbol{u}\right) = \Delta_{\boldsymbol{x}}\boldsymbol{u} - \nabla_{\boldsymbol{x}}p + \delta\gamma\nabla_{\boldsymbol{x}}\cdot\sigma - \delta\left(\int_{S^{d-1}} f\, d\boldsymbol{n}\right)\boldsymbol{e}_2&\\ \nabla_{\boldsymbol{x}}\cdot\boldsymbol{u} = 0&\end{aligned} \tag{2.27}$$

If we express the Navier-Stokes equation in the equivalent form (2.6), then the non-dimensionalized form is given by

$$\begin{aligned}Re\left(\partial_t\boldsymbol{u} + (\boldsymbol{u}\cdot\nabla_{\boldsymbol{x}})\,\boldsymbol{u}\right) = \Delta_{\boldsymbol{x}}\boldsymbol{u} - \nabla_{\boldsymbol{x}}p + \delta\gamma\nabla_{\boldsymbol{x}}\cdot\sigma + \delta\left(1 - \int_{S^{d-1}} f\, d\boldsymbol{n}\right)\boldsymbol{e}_2&\\ \nabla_{\boldsymbol{x}}\cdot\boldsymbol{u} = 0&\end{aligned} \tag{2.28}$$

2.3. Multi-scale mechanism for instability and cluster formation. The multi-scale mechanism that leads to the instability and the formation of clusters was first explained by Koch and Shaqfeh, see [12].

In our kinetic model, the function

$$\rho(\boldsymbol{x},t)=\int_{S^d-1} f(\boldsymbol{x},t,\boldsymbol{n})d\boldsymbol{n}$$

measures the density of rod like particles. By virtue of the buoyancy term in the Stokes equation, a density modulation (as indicated in Figure 2.2 (a)) triggers a modulated shear flow with flow direction $\boldsymbol{e}_2$ (see Fig. 2.2 (b)).

By virtue of the microscopic drift term on the sphere $\nabla_{\boldsymbol{n}}\cdot(P_{\boldsymbol{n}^\perp}\nabla_{\boldsymbol{x}}\boldsymbol{u}\boldsymbol{n}f)$ this shear destroys the uniform distribution f in $\boldsymbol{n}$. For moderate local Deborah numbers the distribution f slightly concentrates in a direction at 45 degrees between the flow direction and the shear direction as shown in Fig. 2.2 (c). For larger shear rates the distribution f concentrates more pronounced in direction of gravity. In this figure we plotted the average microscopic orientation $\lambda\boldsymbol{r}$, where λ is the largest eigenvalue of σ and $\boldsymbol{r}$ is the corresponding eigenvector.

By virtue of the term $-\nabla_{\boldsymbol{x}}\cdot((I+\boldsymbol{n}\otimes\boldsymbol{n})\,\boldsymbol{e}_2 f)$ this nonuniform distribution in $\boldsymbol{n}$ implies that particles on average fall in a direction which is at a non-vanishing angle between flow direction and shear direction. Hence this term acts as a horizontal drift term for the modulated density ρ . In fact, it reinforces the original horizontal modulation of the density ρ since particles with an orientation as shown in Fig. 2.2 (c) move towards the center.

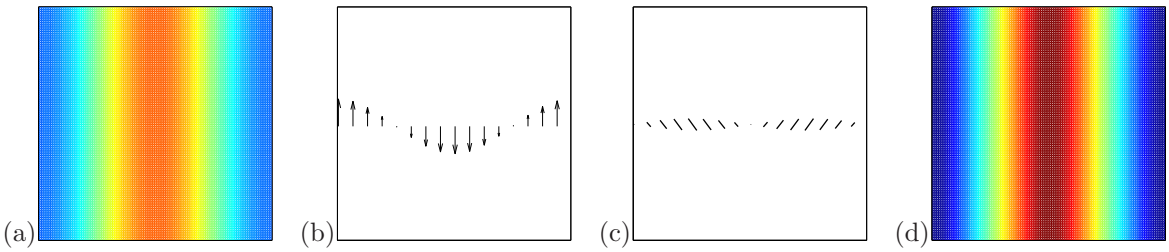

FIG. 2.2. *Illustration of the concentration mechanism (a) initial density modulation, (b) velocity field, (c) microscopic orientation: plot of $\lambda\boldsymbol{r}$, where λ is the largest eigenvalue of σ and $\boldsymbol{r}$ is the corresponding eigenvector, (d) increased density modulation at later time.*

3. Linear stability analysis. Experimental studies for the sedimentation of suspensions with rod-like particles (see [10, 11, 14]) reveal the formations of packets of particles which seem to have a mesoscopic equilibrium width. In our formulation of the problem, this means that the density ρ should acquire variations of a characteristic length scale. Our goal is to give a theoretical explanation of this phenomenon.

Several authors have performed a linear stability analysis ([12, 19]), which however did not predict a wavelength selection mechanism. Instead they found that the infinitesimal growth rate is independent of the wave number $|\boldsymbol{\xi}|$ in the limit $|\boldsymbol{\xi}|\to 0$. Saintillan et al. [18] showed that a small density stratification can lead to a finite wavelength selection. However, the predicted wavelength does not agree with experiments, see [15]. In those papers the Stokes equation was used to model the macroscopic flow. Here we show that the use of the Navier-Stokes equation leads to a wavelength selection mechanism which depends on the dimensionless parameters Re, δ and γ.

In this section we restrict considerations to the spatially two-dimensional case (one horizontal direction + direction of gravity). In this configuration we look at the Smoluchowski equation on S^1 and use the notation $\boldsymbol{x}=(x,y)^t$ and $\boldsymbol{u}=(u,v)^t$. We linearize the Smoluchowski equation around the state $\boldsymbol{u}_0=\boldsymbol{0}$ and $f_0=1/2\pi$ and consider small perturbations of f_0 which we denote by f and perturbations of $\boldsymbol{u}_0$ which we denoted by $\boldsymbol{u}=(u,v)^t$. The evolution of f is described by the equation

$$\partial_t f+\nabla_{\boldsymbol{n}}\cdot(P_{\boldsymbol{n}^\perp}\nabla_{\boldsymbol{x}}\boldsymbol{u}\boldsymbol{n})\,\frac{1}{2\pi}-(D(\boldsymbol{n})\boldsymbol{e}_2)\cdot\nabla_{\boldsymbol{x}}f=\Delta_{\boldsymbol{n}}f+\gamma\nabla_{\boldsymbol{x}}\cdot D(\boldsymbol{n})\nabla_{\boldsymbol{x}}f \tag{3.1}$$

with

$$\boldsymbol{n} = \begin{pmatrix} \cos\theta \\ \sin\theta \end{pmatrix}, \quad D(\boldsymbol{n}) = (I + \boldsymbol{n} \otimes \boldsymbol{n}) = \begin{pmatrix} \cos^2\theta + 1 & \cos\theta\sin\theta \\ \cos\theta\sin\theta & \sin^2\theta + 1 \end{pmatrix}.$$

Now we consider a closure at the level of second moments

$$\rho(\boldsymbol{x},t) := \int_0^{2\pi} f(\boldsymbol{x},\theta,t)\,d\theta, \quad c(\boldsymbol{x},t) := \frac{1}{2}\int_0^{2\pi} \cos(2\theta) f\,d\theta, \quad s(\boldsymbol{x},t) := \frac{1}{2}\int_0^{2\pi} \sin(2\theta) f\,d\theta \tag{3.2}$$

which allows us to derive evolution equations for ρ, c and s, see Appendix A for details. Note that ρ now describes the perturbation of the density. This closure makes sense in the regime where δ is small. In this situation, the velocity gradient caused by modulations in density is small and the rotational diffusion term in the Smoluchowski equation will lead to a fast damping of higher order moments.

The linear model has the form

$$\partial_t\rho = \frac{3}{2}\rho_y - c_y + s_x + \gamma\left(\frac{3}{2}(\rho_{xx}+\rho_{yy}) + 2s_{xy} + c_{xx} - c_{yy}\right) \tag{3.3}$$

$$\partial_t c = -\frac{1}{8}\rho_y + \frac{3}{2}c_y + \frac{1}{4}(u_x - v_y) - 4c + \gamma\Big(\frac{3}{2}\left(c_{xx}+c_{yy}\right) + \frac{1}{8}\left(\rho_{xx}-\rho_{yy}\right)\Big) \tag{3.4}$$

$$\partial_t s = \frac{1}{8}\rho_x + \frac{3}{2}s_y + \frac{1}{4}(u_y + v_x) - 4s + \gamma\left(\frac{1}{4}\rho_{xy} + \frac{3}{2}(s_{xx}+s_{yy})\right). \tag{3.5}$$

In a moving coordinate frame of the form $(\boldsymbol{x'},t') = (\boldsymbol{x} + \frac{3}{2}\boldsymbol{e}_2 t, t)$ we obtain the system (dropping the primes)

$$\partial_t\rho = s_x - c_y + \gamma\left(\frac{3}{2}\left(\rho_{xx}+\rho_{yy}\right) + c_{xx} - c_{yy} + 2s_{xy}\right) \tag{3.6}$$

$$\partial_t c = -\frac{1}{8}\rho_y + \frac{1}{4}\left(u_x - v_y\right) - 4c + \gamma\Big(\frac{1}{8}\left(\rho_{xx}-\rho_{yy}\right) + \frac{3}{2}\left(c_{xx}+c_{yy}\right)\Big) \tag{3.7}$$

$$\partial_t s = \frac{1}{8}\rho_x + \frac{1}{4}\left(u_y + v_x\right) - 4s + \gamma\left(\frac{1}{4}\rho_{xy} + \frac{3}{2}\left(s_{xx}+s_{yy}\right)\right). \tag{3.8}$$

3.1. The Stokes equation. We consider (3.6)-(3.8) together with the Stokes equation ($Re = 0$)

$$\begin{aligned} \Delta u - p_x + \delta\gamma\left(2c_x + 2s_y\right) &= 0 \\ \Delta v - p_y + \delta\gamma\left(2s_x - 2c_y\right) &= \delta\rho \\ u_x + v_y &= 0. \end{aligned} \tag{3.9}$$

Since here ρ is the perturbation of the density, we have on the right hand side the term $\delta\rho$ instead of $\delta(\rho - 1)$ (compare with (2.28)).

We rewrite (3.6)-(3.8) as a system for ρ, $\phi = s_x - c_y$ and $\psi = s_y + c_x$:

$$\begin{aligned} \partial_t\rho &= \phi + \gamma\left(\frac{3}{2}\Delta\rho + \phi_y + \psi_x\right) \\ \partial_t\phi &= \frac{1}{8}\Delta\rho + \frac{1}{4}\Delta v - 4\phi + \gamma\left(\frac{1}{8}\Delta(\rho_y) + \frac{3}{2}\Delta\phi\right) \\ \partial_t\psi &= \frac{1}{4}\Delta u - 4\psi + \gamma\left(\frac{1}{8}\Delta(\rho_x) + \frac{3}{2}\Delta\psi\right). \end{aligned}$$

The terms Δu and Δv are replaced using the Stokes equation, i.e.

$$\begin{aligned} \Delta u &= p_x - \delta\gamma\left(2c_x + 2s_y\right) = p_x - \delta\gamma 2\psi \\ \Delta v &= p_y - \delta\gamma\left(2s_x - 2c_y\right) + \delta\rho = p_y - \delta\gamma 2\phi + \delta\rho. \end{aligned}$$

We obtain the system

$$\begin{aligned}
\partial_t \rho &= \phi + \gamma\left(\frac{3}{2}\Delta\rho + \phi_y + \psi_x\right)\\
\partial_t \phi &= \frac{1}{8}\Delta\rho + \frac{1}{4}\left(p_y - \delta\gamma 2\phi + \delta\rho\right) - 4\phi + \gamma\left(\frac{1}{8}\Delta(\rho_y) + \frac{3}{2}\Delta\phi\right)\\
\partial_t \psi &= \frac{1}{4}\left(p_x - \delta\gamma 2\psi\right) - 4\psi + \gamma\left(\frac{1}{8}\Delta(\rho_x) + \frac{3}{2}\Delta\psi\right).
\end{aligned}$$

After Fourier transformation we obtain with $\boldsymbol{\xi} = (\xi_1, \xi_2)^t$

$$\begin{aligned}
\partial_t \hat{\rho}(\boldsymbol{\xi}, t) &= \hat{\phi}(\boldsymbol{\xi}, t) + \gamma\left(-\frac{3}{2}|\boldsymbol{\xi}|^2\hat{\rho}(\boldsymbol{\xi}, t) + i\xi_2\hat{\phi}(\boldsymbol{\xi}, t) + i\xi_1\hat{\psi}(\boldsymbol{\xi}, t)\right)\\
\partial_t \hat{\phi}(\boldsymbol{\xi}, t) &= -\frac{1}{8}|\boldsymbol{\xi}|^2\hat{\rho}(\boldsymbol{\xi}, t) + \frac{1}{4}i\xi_2\hat{p}(\boldsymbol{\xi}, t) - \frac{1}{2}\delta\gamma\hat{\phi}(\boldsymbol{\xi}, t) + \frac{1}{4}\delta\hat{\rho}(\boldsymbol{\xi}, t)\\
&\quad - 4\hat{\phi}(\boldsymbol{\xi}, t) + \gamma\left(-\frac{1}{8}|\boldsymbol{\xi}|^2 i\xi_2\hat{\rho}(\boldsymbol{\xi}, t) - \frac{3}{2}|\boldsymbol{\xi}|^2\hat{\phi}(\boldsymbol{\xi}, t)\right) \qquad (3.10)\\
\partial_t \hat{\psi}(\boldsymbol{\xi}, t) &= \frac{1}{4}i\xi_1\hat{p} - \frac{1}{2}\delta\gamma\hat{\psi}(\boldsymbol{\xi}, t) - 4\hat{\psi}(\boldsymbol{\xi}, t)\\
&\quad + \gamma\left(-\frac{1}{8}|\boldsymbol{\xi}|^2 i\xi_1\hat{\rho}(\boldsymbol{\xi}, t) - \frac{3}{2}|\boldsymbol{\xi}|^2\hat{\psi}(\boldsymbol{\xi}, t)\right).
\end{aligned}$$

We want to calculate $\hat{p}$ from the Stokes equations. For this we differentiate the first equation of (3.9) with respect to x, the second equation with respect to y and add the two equations. We obtain

$$\Delta\underbrace{(u_x + v_y)}_{=0} - \Delta p + 2\delta\gamma\left(\psi_x + \phi_y\right) = \delta\rho_y.$$

Fourier transformation gives us

$$\hat{p} = -\delta\gamma\frac{2}{|\boldsymbol{\xi}|^2}\left(i\xi_1\hat{\psi} + i\xi_2\hat{\phi}\right) + \delta\frac{i\xi_2}{|\boldsymbol{\xi}|^2}\hat{\rho}. \qquad (3.11)$$

In (3.10) we need expressions for $i\xi_1\hat{p}/4$ and $i\xi_2\hat{p}/4$, which have the form

$$\begin{aligned}
\frac{1}{4}i\xi_1\hat{p} &= \frac{\delta\gamma}{2|\boldsymbol{\xi}|^2}\left(\xi_1^2\hat{\psi} + \xi_1\xi_2\hat{\phi}\right) - \frac{\delta}{4}\frac{\xi_1\xi_2}{|\boldsymbol{\xi}|^2}\hat{\rho}\\
\frac{1}{4}i\xi_2\hat{p} &= \frac{\delta\gamma}{2|\boldsymbol{\xi}|^2}\left(\xi_1\xi_2\hat{\psi} + \xi_2^2\hat{\phi}\right) - \frac{\delta}{4}\frac{\xi_2^2}{|\boldsymbol{\xi}|^2}\hat{\rho}
\end{aligned} \qquad (3.12)$$

Using the expressions (3.12) in (3.10) we obtain the system

$$\begin{aligned}
\partial_t \hat{\phi} &= \hat{\phi}\left(-4 - \frac{3}{2}\gamma|\boldsymbol{\xi}|^2 - \frac{1}{2}\delta\gamma\frac{\xi_1^2}{|\boldsymbol{\xi}|^2}\right) + \hat{\psi}\left(\frac{1}{2}\delta\gamma\frac{\xi_1\xi_2}{|\boldsymbol{\xi}|^2}\right)\\
&\quad + \hat{\rho}\left(-\frac{1}{8}|\boldsymbol{\xi}|^2 + \frac{1}{4}\delta\frac{\xi_1^2}{|\boldsymbol{\xi}|^2} - \frac{1}{8}\gamma i\xi_2|\boldsymbol{\xi}|^2\right)\\
\partial_t \hat{\psi} &= \hat{\phi}\left(\frac{1}{2}\delta\gamma\frac{\xi_1\xi_2}{|\boldsymbol{\xi}|^2}\right) + \hat{\psi}\left(-4 - \frac{3}{2}\gamma|\boldsymbol{\xi}|^2 - \frac{1}{2}\delta\gamma\frac{\xi_2^2}{|\boldsymbol{\xi}|^2}\right) \qquad (3.13)\\
&\quad + \hat{\rho}\left(-\frac{1}{4}\delta\frac{\xi_1\xi_2}{|\boldsymbol{\xi}|^2} - \frac{1}{8}\gamma i\xi_1|\boldsymbol{\xi}|^2\right)\\
\partial_t \hat{\rho} &= \hat{\phi}\left(1 + \gamma i\xi_2\right) + \hat{\psi}\left(\gamma i\xi_1\right) + \hat{\rho}\left(-\frac{3}{2}\gamma|\boldsymbol{\xi}|^2\right)
\end{aligned}$$

We have rewritten the problem into a linear ODE system of the form

$$\partial_t \boldsymbol{U}(\boldsymbol{\xi}, t) = A(\boldsymbol{\xi}, \delta, \gamma)\boldsymbol{U}(\boldsymbol{\xi}, t),$$

with $\boldsymbol{U}(\boldsymbol{\xi},t) = \left(\hat{\phi},\hat{\psi},\hat{\rho}\right)^T$ and $A(\boldsymbol{\xi},\delta,\gamma)$ equal to

$$\begin{pmatrix} -4-\frac{3}{2}\gamma|\boldsymbol{\xi}|^2-\frac{1}{2}\delta\gamma\frac{\xi_1^2}{|\boldsymbol{\xi}|^2} & \frac{1}{2}\delta\gamma\frac{\xi_1\xi_2}{|\boldsymbol{\xi}|^2} & -\frac{1}{8}|\boldsymbol{\xi}|^2+\frac{1}{4}\delta\frac{\xi_1^2}{|\boldsymbol{\xi}|^2}-\frac{1}{8}\gamma i\xi_2|\boldsymbol{\xi}|^2 \\ \frac{1}{2}\delta\gamma\frac{\xi_1\xi_2}{|\boldsymbol{\xi}|^2} & -4-\frac{3}{2}\gamma|\boldsymbol{\xi}|^2-\frac{1}{2}\delta\gamma\frac{\xi_2^2}{|\boldsymbol{\xi}|^2} & -\frac{1}{4}\delta\frac{\xi_1\xi_2}{|\boldsymbol{\xi}|^2}-\frac{1}{8}\gamma i\xi_1|\boldsymbol{\xi}|^2 \\ 1+\gamma i\xi_2 & \gamma i\xi_1 & -\frac{3}{2}\gamma|\boldsymbol{\xi}|^2 \end{pmatrix}$$

With $\alpha(A)$ we denote the spectral abscissa, which is defined by

$$\alpha(A) := \max_{1\le j\le 3} \mathrm{Re}(\lambda_j),$$

where λ_j, $j = 1,2,3$ are the eigenvalues of A. Now $\boldsymbol{U}(\boldsymbol{\xi},t)$ remains bounded provided $\alpha(A) \le 0$ and $\boldsymbol{U}(\boldsymbol{\xi},t) \to 0$ as $t \to \infty$ if $\alpha(A) < 0$.

In Figure 3.1 we show plots of the positive part of the spectral abscissa for different values of δ and γ. Since we can not give analytical expressions of the eigenvalues of the matrix A, we calculated (using

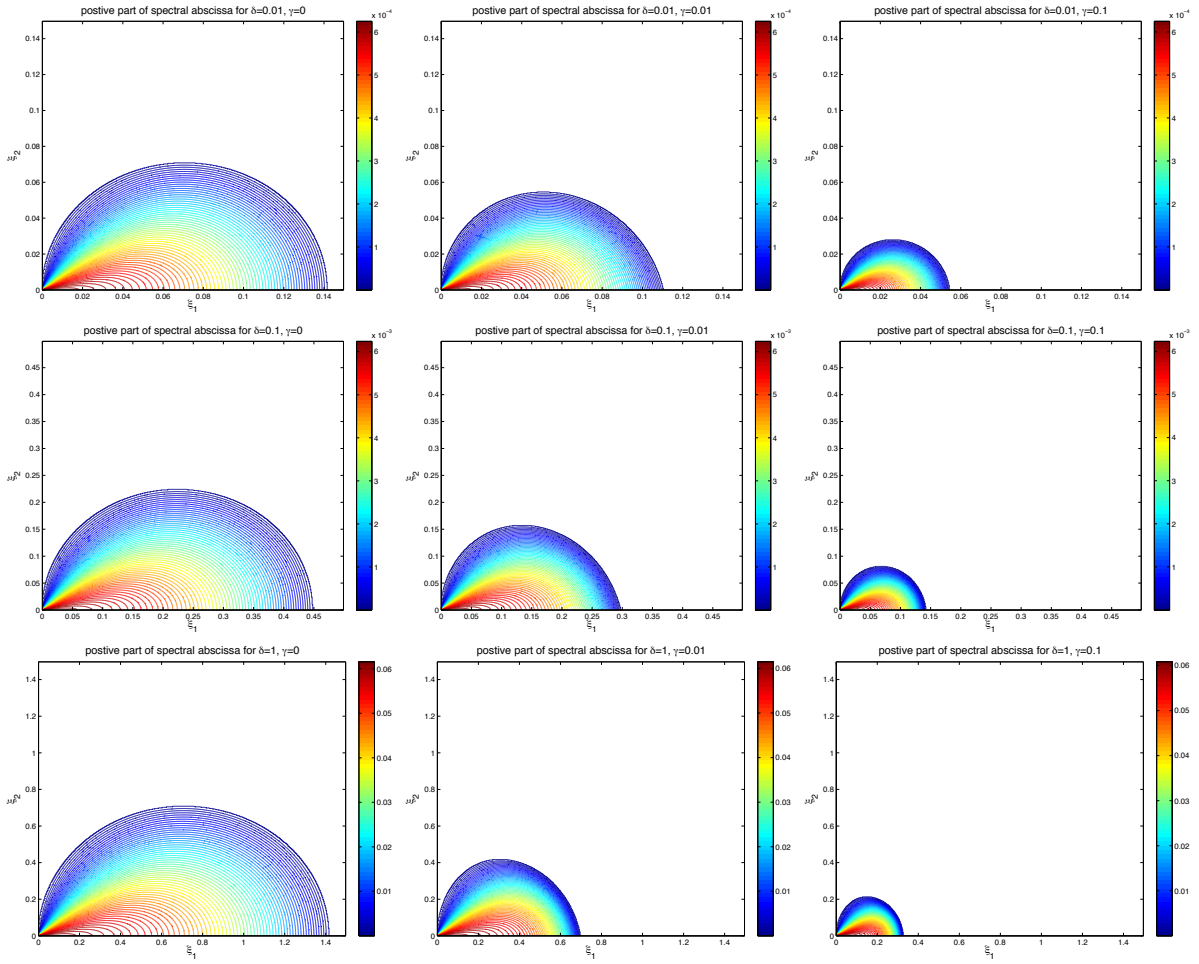

FIG. 3.1. *Positive part of spectral abscissa for the matrix A vs. ξ_1 and ξ_2 for different values of δ and γ.*

MATLAB) the positive part of the spectral abscissa on a fine mesh in the ξ_1-ξ_2-plane. We summarize our observations in Remark 3.1.

REMARK 3.1. *On the level of linear instability, there is no wavelength selection mechanism for the coupled micro-macro model with the macroscopic Stokes equation.*

An increase of the parameter δ has a destabilizing effect, while an increase of the parameter γ has a stabilizing effect.

3.2. The Navier-Stokes equation. We now study the linear stability for the system (3.3)-(3.5) together with the Navier-Stokes equation

$$Re\partial_t u = u_{xx} + u_{yy} - p_x + \delta\gamma 2\left(c_x + s_y\right) \tag{3.14}$$
$$Re\partial_t v = v_{xx} + v_{yy} - p_y + \delta\gamma 2\left(s_x - c_y\right) - \delta\rho. \tag{3.15}$$

Since we linearize around the velocity $\boldsymbol{u}_0 = 0$, the effect of the convective term is neglected. Note that we here use the linear moment closure system in the non-moving frame (instead of transforming the Navier-Stokes equation to the moving coordinate system).

A Fourier transformation of (3.3)-(3.5), (3.14), (3.15) leads to the system

$$\partial_t\hat{\rho} = \frac{3}{2}i\xi_2\hat{\rho} + i\xi_1\hat{s} - i\xi_2\hat{c} + \gamma\left(-\frac{3}{2}|\boldsymbol{\xi}|^2\hat{\rho} - \xi_1^2\hat{c} + \xi_2^2\hat{c} - 2\xi_1\xi_2\hat{s}\right) \tag{3.16}$$
$$\partial_t\hat{c} = -\frac{1}{8}i\xi_2\hat{\rho} + \frac{3}{2}i\xi_2\hat{c} + \frac{1}{4}\left(i\xi_1\hat{u} - i\xi_2\hat{v}\right) - 4\hat{c} + \gamma\left(\frac{1}{8}\left(-\xi_1^2\hat{\rho} + \xi_2^2\hat{\rho}\right) - \frac{3}{2}|\boldsymbol{\xi}|^2\hat{c}\right) \tag{3.17}$$
$$\partial_t\hat{s} = \frac{1}{8}i\xi_1\hat{\rho} + \frac{3}{2}i\xi_2\hat{s} + \frac{1}{4}\left(i\xi_2\hat{u} + i\xi_1\hat{v}\right) - 4\hat{s} + \gamma\big(-\frac{1}{4}\xi_1\xi_2\hat{\rho} - \frac{3}{2}|\boldsymbol{\xi}|^2\hat{s}\big) \tag{3.18}$$
$$\partial_t\hat{u} = \frac{1}{Re}\left(-|\boldsymbol{\xi}|^2\hat{u} - i\xi_1\hat{p} + 2\delta\gamma\left(i\xi_1\hat{c} + i\xi_2\hat{s}\right)\right) \tag{3.19}$$
$$\partial_t\hat{v} = \frac{1}{Re}\left(-|\boldsymbol{\xi}|^2\hat{v} - i\xi_2\hat{p} + 2\delta\gamma\left(i\xi_1\hat{s} - i\xi_2\hat{c}\right) - \delta\hat{\rho}\right) \tag{3.20}$$

We eliminate the pressure term $\hat{p}$ using the expression

$$\hat{p} = \frac{2\delta\gamma}{|\boldsymbol{\xi}|^2}\left(2\xi_1\xi_2\hat{s} + \xi_1^2\hat{c} - \xi_2^2\hat{c}\right) + \frac{\delta}{|\boldsymbol{\xi}|^2}i\xi_2\hat{\rho}. \tag{3.21}$$

Equations (3.19) and (3.20) can thus be written in the form

$$\partial_t\hat{u} = \frac{1}{Re}\left(\delta\frac{\xi_1\xi_2}{|\boldsymbol{\xi}|^2}\hat{\rho} - |\boldsymbol{\xi}|^2\hat{u} + 2\delta\gamma\xi_2 i\left(1 - \frac{2\xi_1^2}{|\boldsymbol{\xi}|^2}\right)\hat{s} + \frac{4\delta\gamma i\xi_1\xi_2^2}{|\boldsymbol{\xi}|^2}\hat{c}\right) \tag{3.22}$$
$$\partial_t\hat{v} = \frac{1}{Re}\left(-\delta\frac{\xi_1^2}{|\boldsymbol{\xi}|^2}\hat{\rho} - |\boldsymbol{\xi}|^2\hat{v} + 2\delta\gamma\xi_1 i\left(1 - \frac{2\xi_2^2}{|\boldsymbol{\xi}|^2}\right)\hat{s} - \frac{4\delta\gamma\xi_2 i\xi_1^2}{|\boldsymbol{\xi}|^2}\hat{c}\right) \tag{3.23}$$

We have rewritten the problem into a linear ODE system of the form

$$\partial_t\boldsymbol{U}(\boldsymbol{\xi},t) = A(\boldsymbol{\xi},\delta,\gamma,Re)\boldsymbol{U}(\boldsymbol{\xi},t),$$

with $\boldsymbol{U}(\boldsymbol{\xi},t) = (\hat{\rho},\hat{c},\hat{s},\hat{u},\hat{v})^t$ and A equal to

$$\begin{pmatrix}
-\frac{3}{2}\gamma|\boldsymbol{\xi}|^2 + \frac{3}{2}i\xi_2 & -i\xi_2 + \gamma(\xi_2^2 - \xi_1^2) & i\xi_1 - 2\gamma\xi_1\xi_2 & 0 & 0 \\
\frac{1}{8}\left(-i\xi_2 + \gamma(\xi_2^2 - \xi_1^2)\right) & -4 - \frac{3}{2}\gamma|\boldsymbol{\xi}|^2 + \frac{3}{2}i\xi_2 & 0 & \frac{1}{4}i\xi_1 & -\frac{1}{4}i\xi_2 \\
\frac{1}{8}i\xi_1 - \frac{1}{4}\gamma\xi_1\xi_2 & 0 & -4 - \frac{3}{2}\gamma|\boldsymbol{\xi}|^2 + \frac{3}{2}i\xi_2 & \frac{1}{4}i\xi_2 & \frac{1}{4}i\xi_1 \\
\frac{\delta\xi_1\xi_2}{Re|\boldsymbol{\xi}|^2} & \frac{4\delta\gamma i\xi_1\xi_2^2}{Re|\boldsymbol{\xi}|^2} & \frac{2\delta\gamma i\xi_2}{Re}\left(1 - \frac{2\xi_1^2}{|\boldsymbol{\xi}|^2}\right) & -\frac{|\boldsymbol{\xi}|^2}{Re} & 0 \\
-\frac{\delta\xi_1^2}{Re|\boldsymbol{\xi}|^2} & -\frac{4\delta\gamma i\xi_2\xi_1^2}{Re|\boldsymbol{\xi}|^2} & \frac{2\delta\gamma i\xi_1}{Re}\left(1 - \frac{2\xi_2^2}{|\boldsymbol{\xi}|^2}\right) & 0 & -\frac{|\boldsymbol{\xi}|^2}{Re}
\end{pmatrix}$$

In Figures 3.2, 3.3 we plot the positive part of the spectral abscissa for different choices of the parameter values Re, δ and γ.

REMARK 3.2. *For the coupled micro-macro model with the Navier-Stokes equation, the linear stability analysis predicts a wavelength selection which depends on Re, δ and γ. An increase of Re decreases the wavelength of the most unstable configuration. An increase of δ has a destabilizing effect and decreases the wavelength of the most unstable wave. An increase of γ has a stabilizing effect and increases the wavelength of the most unstable wave.*

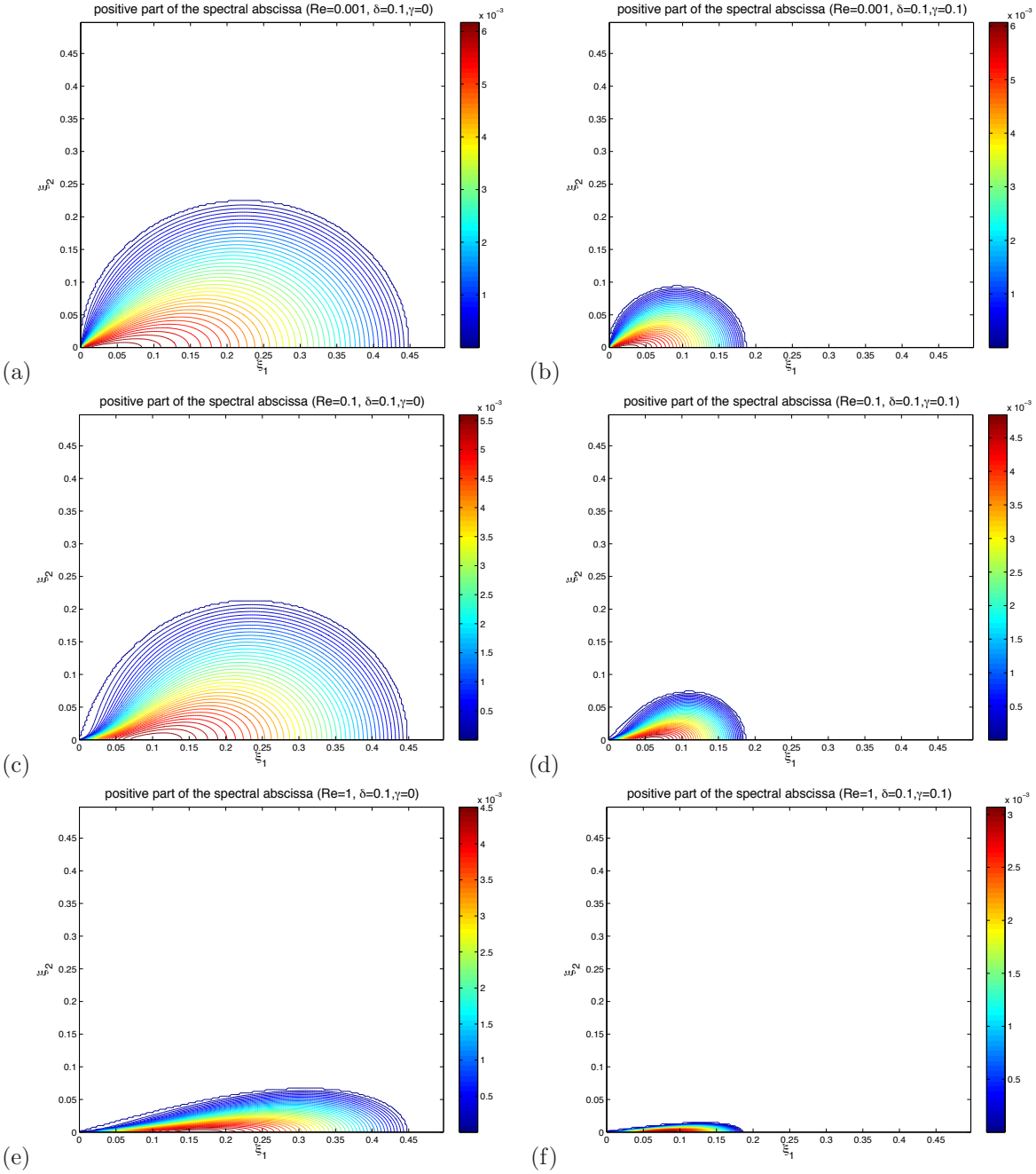

FIG. 3.2. *Positive part of the spectral abscissa for* $\delta = 0.1$ *and different values of the parameter values Re and* γ.

3.3. Asymptotic expansion of the relevant eigenvalue. It is expected that the most unstable wavelength lies in the nearly horizontal direction. This motivates to consider the special case $\xi_2 = 0$ and (for simplicity) $\gamma = 0$. We give an asymptotic expansion of the unstable eigenvalue of the linearized system in *Re*. This asymptotic expansion captures the singular effect of the dependence on the Reynolds number and explains why the inclusion of inertial effects leads to a wavelength selection.

PROPOSITION 3.1. *Consider horizontal waves in the regime* $\gamma = 0$. *For* $Re = 0$, *the coupled system is linearly stable provided that the eigenvalue*

$$\lambda_0 = \frac{1}{4}\left(-8 + \sqrt{64 + 4\delta - 2\xi_1^2}\right)$$

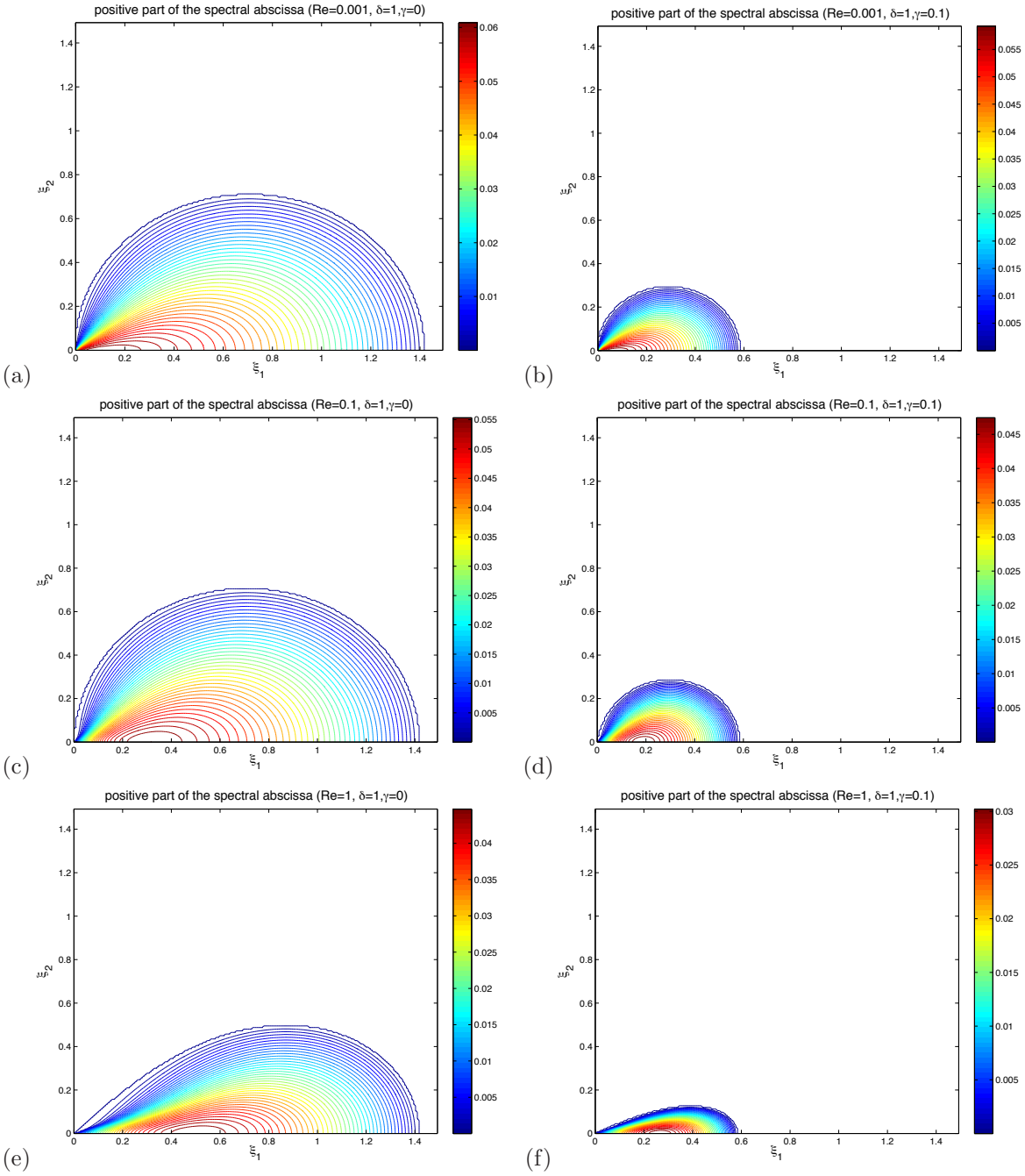

FIG. 3.3. *Positive part of the spectral abscissa for $\delta = 1$ and different values of the parameter values Re and γ.*

is smaller than zero, otherwise it is unstable.

For $Re > 0$ (and $Re \ll 1$) the change of this eigenvalue can be described by an asymptotic expansion of the form

$$\lambda = \lambda_0 + (Re)\lambda_1 + \dots$$

with

$$\lambda_1 = -\frac{\delta}{\frac{2\xi_1^2}{(2\delta-\xi_1^2)}\left(8+\sqrt{64+4\delta-2\xi_1^2}\right)^2 + 4\xi_1^2}.$$

Proof: Our starting point is the linear system which is obtained via Fourier transformation of the linear moment closure. For $\xi_2 = 0$, $\gamma = 0$, this system has the form (dropping all the hats)

$$\begin{aligned} \partial_t \rho &= i\xi_1 s \\ \partial_t c &= \frac{1}{4} i\xi_1 u - 4c \\ \partial_t s &= \frac{1}{8} i\xi_1 \rho + \frac{1}{4} i\xi_1 v - 4s \end{aligned} \tag{3.24}$$

Using the notation $\boldsymbol{x} = (\rho, c, s)^T$, $\boldsymbol{y} = (u, v)^T$, we rewrite (3.24) into the form

$$\dot{\boldsymbol{x}} = A\boldsymbol{x} + B\boldsymbol{y}, \tag{3.25}$$

with

$$A = \begin{pmatrix} 0 & 0 & i\xi_1 \\ 0 & -4 & 0 \\ \frac{1}{8} i\xi_1 & 0 & -4 \end{pmatrix}, \quad B = \begin{pmatrix} 0 & 0 \\ \frac{1}{4} i\xi_1 & 0 \\ 0 & \frac{1}{4} i\xi_1 \end{pmatrix}.$$

From the Stokes equation ($Re = 0$) we obtain

$$\begin{aligned} -\xi_1^2 u &= 0 \\ -\xi_1^2 v - \delta\rho &= 0, \end{aligned}$$

which we rewrite into the form

$$0 = C\boldsymbol{y} + D\boldsymbol{x}, \tag{3.26}$$

with

$$C = \begin{pmatrix} -\xi_1^2 & 0 \\ 0 & -\xi_1^2 \end{pmatrix}, \quad D = \begin{pmatrix} 0 & 0 & 0 \\ -\delta & 0 & 0 \end{pmatrix}.$$

Using (3.26), we obtain $\boldsymbol{y} = -C^{-1}D\boldsymbol{x}$. Introducing this in (3.25) gives

$$\dot{\boldsymbol{x}} = \left(A - BC^{-1}D\right)\boldsymbol{x}. \tag{3.27}$$

The eigenvalues of $(A - BC^{-1}D)$ are

$$\left\{-4,\ \frac{1}{4}\left(-8 - \sqrt{64 + 4\delta - 2\xi_1^2}\right),\ \frac{1}{4}\left(-8 + \sqrt{64 + 4\delta - 2\xi_1^2}\right)\right\}. \tag{3.28}$$

The last eigenvalue (which we denote by λ_0) is larger than zero provided that $\delta > 0$ and ξ_1^2 is small enough. Thus, for horizontal waves and $\gamma = 0$, the moment closure system coupled with the Stokes equation is most unstable for waves with wave number $\xi_1 \to 0$, compare with Figure 3.1 (left column).

The eigenvector corresponding to the eigenvalue λ_0 has the form

$$\boldsymbol{x}_0 = \left(\frac{2i\xi_1}{2\delta - \xi_1^2}\left(8 + \sqrt{64 + 4\delta - 2\xi_1^2}\right), 0, 1\right)^T. \tag{3.29}$$

Now we consider the case $Re > 0$, for which the linearized coupled system can be expressed in the form

$$\begin{pmatrix} \dot{\boldsymbol{x}} \\ \dot{\boldsymbol{y}} \end{pmatrix} = \begin{pmatrix} A & B \\ \frac{1}{Re} D & \frac{1}{Re} C \end{pmatrix} \begin{pmatrix} \boldsymbol{x} \\ \boldsymbol{y} \end{pmatrix}. \tag{3.30}$$

Our goal is to give an asymptotic expansion for eigenvalues of the matrix arising on the right hand side of (3.30), which is valid for small values of Re. In particular we wish to understand how the eigenvalue λ_0 changes with Re. We make the ansatz

$$\begin{aligned} A\boldsymbol{x}_\varepsilon + B\boldsymbol{y}_\varepsilon &= \lambda_\varepsilon \boldsymbol{x}_\varepsilon \\ C\boldsymbol{y}_\varepsilon + D\boldsymbol{x}_\varepsilon &= \varepsilon\lambda_\varepsilon \boldsymbol{y}_\varepsilon, \end{aligned} \tag{3.31}$$

with

$$\begin{aligned} \lambda_\varepsilon &= \lambda_0 + \varepsilon\lambda_1 + \dots \\ \boldsymbol{x}_\varepsilon &= \boldsymbol{x}_0 + \varepsilon\boldsymbol{x}_1 + \dots \\ \boldsymbol{y}_\varepsilon &= \boldsymbol{y}_0 + \varepsilon\boldsymbol{y}_1 + \dots . \end{aligned}$$

We obtain

$\mathcal{O}(1)$: (as considered above)

$$\begin{aligned} A\boldsymbol{x}_0 + B\boldsymbol{y}_0 &= \lambda_0 \boldsymbol{x}_0 \\ C\boldsymbol{y}_0 + D\boldsymbol{x}_0 &= 0 \end{aligned} \tag{3.32}$$

$\mathcal{O}(\varepsilon)$:

$$\begin{aligned} A\boldsymbol{x}_1 + B\boldsymbol{y}_1 &= \lambda_0\boldsymbol{x}_1 + \lambda_1\boldsymbol{x}_0 \\ C\boldsymbol{y}_1 + D\boldsymbol{x}_1 &= \lambda_0\boldsymbol{y}_0, \end{aligned} \tag{3.33}$$

which we rewrite into the form

$$\begin{pmatrix} A-\lambda_0 I & B \\ D & C \end{pmatrix} \begin{pmatrix} \boldsymbol{x}_1 \\ \boldsymbol{y}_1 \end{pmatrix} = \begin{pmatrix} \lambda_1\boldsymbol{x}_0 \\ \lambda_0\boldsymbol{y}_0 \end{pmatrix}. \tag{3.34}$$

The left null space of the matrix on the left hand side of (3.34) is given by

$$\boldsymbol{u}^T = \left(-8 - \sqrt{64+4\delta-2\xi_1^2}, 0, -4i\xi_1, 0, 1\right). \tag{3.35}$$

We multiply both sides of Equation (3.34) from the left with $\boldsymbol{u}^T$ and obtain

$$0 = \boldsymbol{u}^T \cdot \begin{pmatrix} \lambda_1\boldsymbol{x}_0 \\ \lambda_0\boldsymbol{y}_0 \end{pmatrix}. \tag{3.36}$$

Here

$$\boldsymbol{y}_0 = -C^{-1}D\boldsymbol{x}_0 = -\begin{pmatrix} 0 \\ \frac{2\delta i}{\xi_1}\frac{(8+\sqrt{64+4\delta-2\xi_1^2})}{2\delta-\xi_1^2} \end{pmatrix}.$$

Using the expressions for λ_0, $\boldsymbol{x}_0$, $\boldsymbol{y}_0$ and $\boldsymbol{u}$ in Equation (3.36), we can now calculate λ_1, which has the form

$$\lambda_1 = -\frac{\delta}{\frac{2\xi_1^2}{(2\delta-\xi_1^2)}\left(8+\sqrt{64+4\delta-2\xi_1^2}\right)^2 + 4\xi_1^2}. \tag{3.37}$$

In Figure 3.4 we show a plot of λ calculated by the asymptotic expansion (solid line) and compare it with the positive part of the spectral abscissa (calculated at discrete points) for purely horizontal waves.

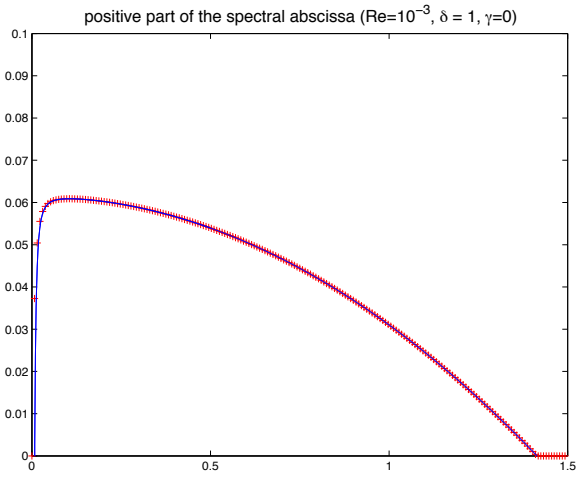

FIG. 3.4. *Solid line: eigenvalue calculated from asymptotic expansion, '+'-symbol: positive part of spectral abscissa for* $Re = 0.001$ *and* $\delta = 1$.

3.4. Numerical simulations of the nonlinear model. Here we show numerical simulations for the system

$$\begin{aligned} \partial_t f + \partial_\theta \left(v_x \cos^2\theta f \right) - \partial_x \left(\sin\theta \cos\theta f \right) &= \partial_{\theta\theta} f \\ \partial_t v &= v_{xx} + \delta \left(1 - \int_{S^1} f d\theta \right), \end{aligned} \tag{3.38}$$

i.e. we solve the coupled model in a simple setting with

$$\boldsymbol{u} = \begin{pmatrix} 0 \\ v(x,t) \\ 0 \end{pmatrix}, \quad f = f(x,\theta,t),$$

We use $\delta = 1$ (and $\gamma = 0$, $Re = 1$).

Initial values are specified on an interval of length $L = 500$, periodicity is assumed. The initial values for f have the form

$$f(x,0,\theta) = \frac{1}{2\pi} + p(x) \quad x \in [0,L), \ \forall\theta \tag{3.39}$$

where $p(x)$ is a small perturbation with size of the order 5×10^{-7}, see Figure 3.5. The velocity v is initially set to zero.

We discretize the macroscopic domain by 8000 grid cells. At each grid point of the macroscopic domain we discretize the Smoluchowski equation on S^1 using 100 grid cells.

In Figure 3.6 we show numerical simulations for the nonlinear initial value problem. In 3.6 (a) we show a plot of f as a function of x (horizontal axis) and θ (vertical axis), (b) shows a plot of ρ. The results of a discrete Fourier transformation of $\rho - 1$ as a function of $|\boldsymbol{\xi}| = |\xi_1|$ are shown in Figure 3.6 (c), (d). The numerical result obtained for the nonlinear model fits well to the prediction of the linear theory, compare with Figure 3.3 (e). Instabilities are only observed within the domain predicted by the linear theory. Furthermore, the most unstable waves are observed for wave number $|\xi_1| \approx 0.5$.

In Figure 3.7 we show plots of the density ρ at later times. We observe regions with high concentration which are separated by regions with very small concentration of particles. This is the nonlinear regime, the solution structure can no longer be predicted by a linearized model. In Section 5 we show that for a particular scaling of our model the evolution of ρ can be described by a Keller-Segel model.

4. Sedimentation of non-Brownian particles. In experimental and numerical studies that can be found in the literature (e.g. [14, 17]), the authors discuss the sedimentation for suspensions of

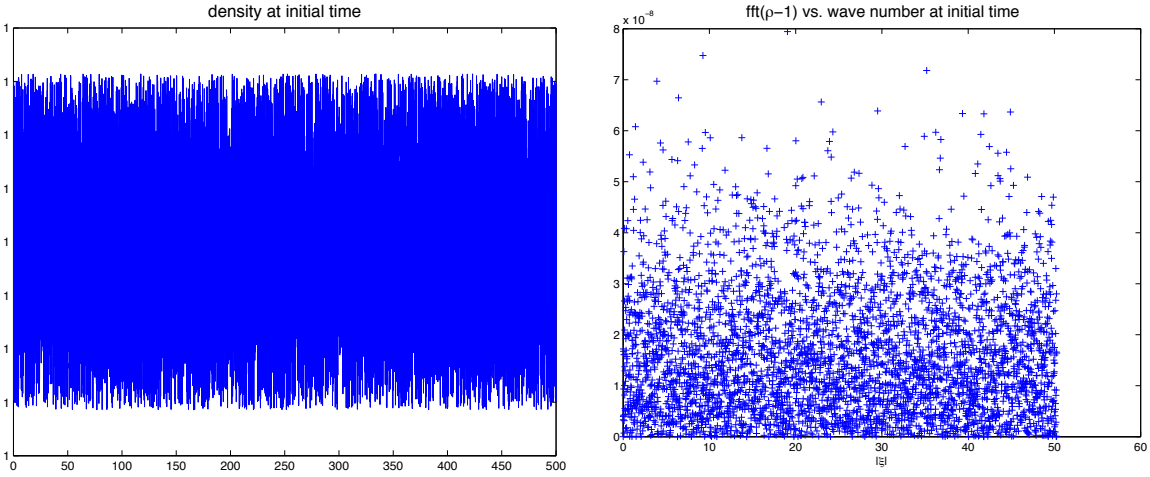

FIG. 3.5. *Initial values of density ρ and $fft(\rho - 1)$.*

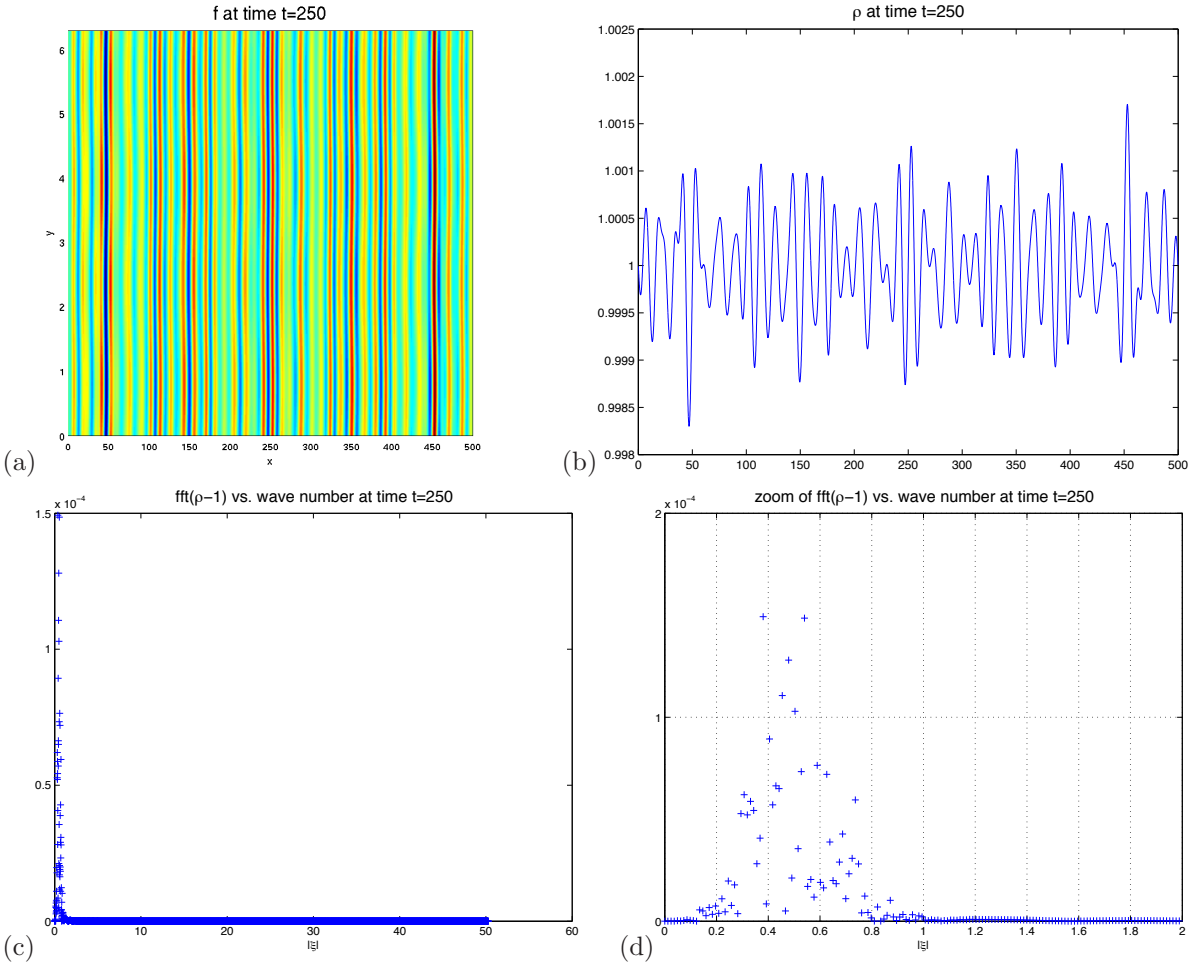

FIG. 3.6. *Numerical results for the initial value problem (3.38), (3.39) at time $t = 250$. (a) $f(\theta, x)$, (b) $\rho(x)$, (c) $fft(\rho - 1)$ vs. $|\xi_1|$, (d) closeup view of results from Fourier transformation.*

non-Brownian particles. For our kinetic model, this case can be considered by setting the absolute

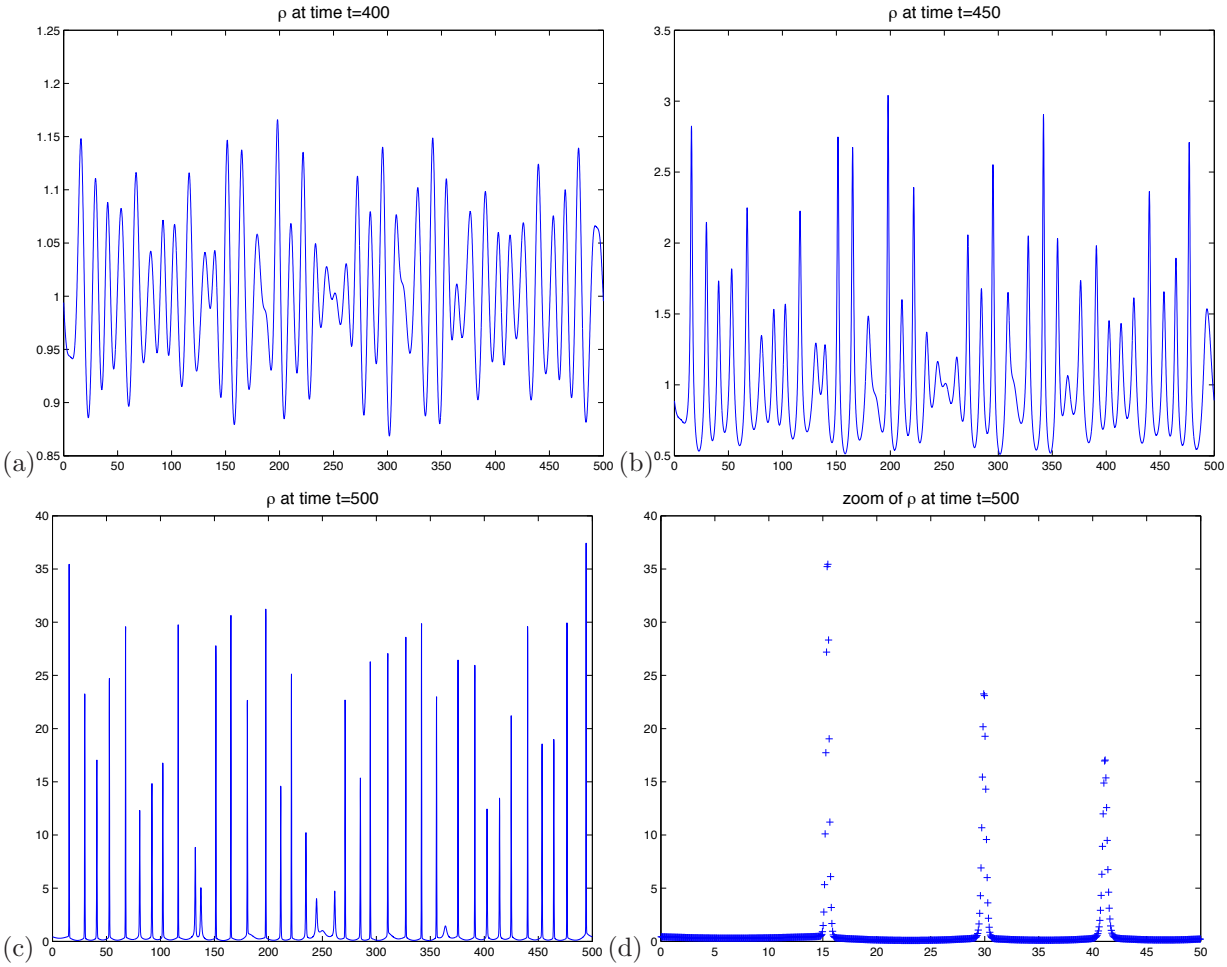

FIG. 3.7. *Numerical results for the initial value problem (3.38) at later times. Figure (d) showes a closeup view of the solution from (c)*

temperature equal to zero. We then obtain the system

$$\begin{aligned} \partial_t f &= -\nabla_{\boldsymbol{x}} \cdot (\boldsymbol{u} f) - \nabla_{\boldsymbol{n}} \cdot (P_{\boldsymbol{n}^\perp} \nabla_{\boldsymbol{x}} \boldsymbol{u} \boldsymbol{n} f) + \frac{m_0 g}{\zeta_\perp} \nabla_{\boldsymbol{x}} \cdot (D(\boldsymbol{n}) \boldsymbol{e}_2 f) \\ \rho_f \left(\partial_t \boldsymbol{u} + (\boldsymbol{u} \cdot \nabla_{\boldsymbol{x}}) \boldsymbol{u}\right) &= \mu \Delta \boldsymbol{u} - \nabla_{\boldsymbol{x}} p + \left(\frac{N}{V} - \int_{S^2} f d\boldsymbol{n}\right) m_0 g \boldsymbol{e}_2 \\ 0 &= \nabla_{\boldsymbol{x}} \cdot \boldsymbol{u}. \end{aligned} \tag{4.1}$$

In order to non-dimensionalize the system we consider a scaling of the form

$$t = T\hat{t},\ \boldsymbol{x} = X\hat{\boldsymbol{x}},\ \boldsymbol{u} = \frac{X}{T}\hat{\boldsymbol{u}},\ f = \frac{N}{V}\hat{f},\ p = \frac{\mu}{T}\hat{p}.$$

where $V = O(L^3)$ is the volume occupied by the suspension, and L is the size of the macroscopic domain. Time and space scales are selected according to

$$T = \frac{m_0}{\zeta_\perp} \quad \text{and} \quad X = \frac{m_0^2 g}{\zeta_\perp^2}, \tag{4.2}$$

which corresponds to the velocity scale (2.20). We obtain the non-dimensional equations (dropping all the hats)

$$\begin{aligned} \partial_t f &= -\nabla_{\boldsymbol{x}} \cdot (\boldsymbol{u} f) - \nabla_{\boldsymbol{n}} \cdot (P_{\boldsymbol{n}^\perp} \nabla_{\boldsymbol{x}} \boldsymbol{u} \boldsymbol{n} f) + \nabla_{\boldsymbol{x}} \cdot (D(\boldsymbol{n}) \boldsymbol{e}_2 f) \\ Re\left(\partial_t \boldsymbol{u} + (\boldsymbol{u} \cdot \nabla_{\boldsymbol{x}})\, \boldsymbol{u}\right) &= \Delta_{\boldsymbol{x}} \boldsymbol{u} - \nabla_{\boldsymbol{x}} p + \delta \left(1 - \int_{S^2} f d\boldsymbol{n}\right) \boldsymbol{e}_2 \\ 0 &= \nabla_{\boldsymbol{x}} \cdot \boldsymbol{u}, \end{aligned} \tag{4.3}$$

with non-dimensional parameters $Re = \rho_f \frac{X^2}{\mu T}$ and $\delta = \frac{N}{V} \frac{m_0 g T X}{\mu}$.

In analogy to the previous section, we now present a linear stability analysis for this slightly simpler model. By neglecting diffusion there is no justification to restrict considerations to second order moments, since there is no fast damping of higher moments. However, our numerical simulations of the nonlinear model will show good agreement with the wavelength selection mechanism predicted by the linear model.

We consider the spatially two-dimensional case and linearize around the state $\boldsymbol{u}_0 = 0$ and $f_0 = \frac{1}{2\pi}$, f and $\boldsymbol{u}$ now denote small perturbations of f_0 and $\boldsymbol{u}_0$. The linearized equations have the form

$$\begin{aligned} \partial_t f &= -\nabla_{\boldsymbol{n}} \cdot (P_{\boldsymbol{n}^\perp} \nabla_{\boldsymbol{x}} \boldsymbol{u} \boldsymbol{n}) \frac{1}{2\pi} + (D(\boldsymbol{n}) \boldsymbol{e}_2) \cdot \nabla_{\boldsymbol{x}} f \\ Re \partial_t \boldsymbol{u} &= \Delta_{\boldsymbol{x}} \boldsymbol{u} - \nabla_{\boldsymbol{x}} p - \delta \left(\int_{S^2} f d\boldsymbol{n}\right) \boldsymbol{e}_2. \end{aligned} \tag{4.4}$$

We consider a moment closure on the level of ρ, c, s as defined in (3.2) and obtain the evolution equations

$$\begin{aligned} \partial_t \rho &= s_x + \frac{3}{2}\rho_y - c_y \\ \partial_t c &= \frac{3}{2} c_y - \frac{1}{8}\rho_y + \frac{1}{4}(u_x - v_y) \\ \partial_t s &= \frac{1}{8}\rho_x + \frac{3}{2} s_y + \frac{1}{4}(u_y + v_x). \end{aligned} \tag{4.5}$$

By changing to a moving coordinate system, we get

$$\begin{aligned} \partial_t \rho &= s_x - c_y \\ \partial_t c &= -\frac{1}{8}\rho_y + \frac{1}{4}(u_x - v_y) \\ \partial_t s &= \frac{1}{8}\rho_x + \frac{1}{4}(u_y + v_x). \end{aligned} \tag{4.6}$$

We first consider the system (4.6) together with the Stokes equation

$$\begin{aligned} \Delta u - p_x &= 0 \\ \Delta v - p_y &= \delta\rho \\ u_x + v_y &= 0. \end{aligned} \tag{4.7}$$

Using $\phi = s_x - c_y$, we can rewrite (4.6) into the form

$$\begin{aligned} \partial_t \rho &= \phi \\ \partial_t \phi &= \frac{1}{8}\Delta\rho + \frac{1}{4}\Delta v, \end{aligned}$$

and by using (4.7) we obtain

$$\begin{aligned} \partial_t \rho &= \phi \\ \partial_t \phi &= \frac{1}{8}\Delta\rho + \frac{1}{4}(\delta\rho + p_y). \end{aligned}$$

Using Fourier transformation and elimination of the pressure term, we derive the linear ode system

$$\partial_t \begin{pmatrix} \hat{\rho} \\ \hat{\phi} \end{pmatrix} = \begin{pmatrix} 0 & 1 \\ -\frac{1}{8}|\boldsymbol{\xi}|^2 + \frac{1}{4}\delta\frac{\xi_1^2}{|\boldsymbol{\xi}|^2} & 0 \end{pmatrix} \begin{pmatrix} \hat{\rho} \\ \hat{\phi} \end{pmatrix}. \tag{4.8}$$

In Figure 4.1, we plot contour lines in the $\xi_1 - \xi_2$-plane for the positive part of the spectral abscissa for the matrix on the right hand side of equation (4.8). At the level of linear stability analysis there is

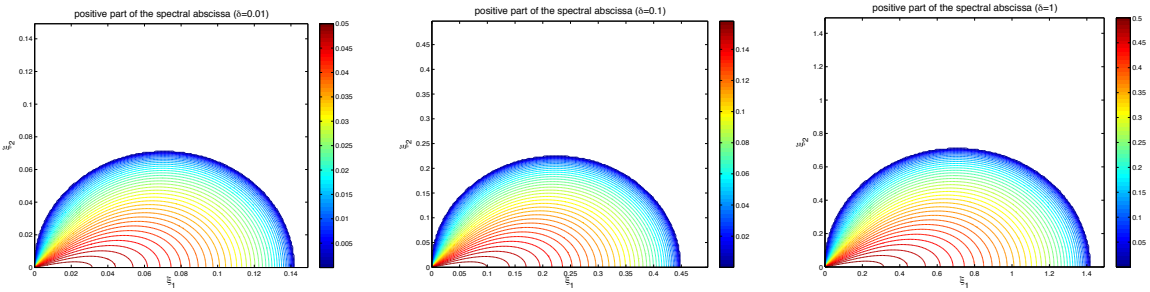

FIG. 4.1. *Positive part of spectral abscissa for the matrix arising in the linear stability analysis of the system modeling the sedimentation of non-Brownian particles in a Stokes flow (with* $\delta = 0.01, 0.1, 1$*).*

no wavelength selection mechanism for the micro-macro model (4.3) with $Re = 0$. An increase of the parameter δ has a destabilizing effect.

We now consider system (4.5) together with the linearized Navier-Stokes equation

$$\begin{aligned} Re\partial_t u &= \Delta u - p_x \\ Re\partial_t v &= \Delta v - p_y - \delta\rho \\ 0 &= u_x + v_y. \end{aligned} \tag{4.9}$$

Fourier transformation and elimination of the pressure leads to the linear ode system

$$\partial_t \begin{pmatrix} \hat{\rho} \\ \hat{c} \\ \hat{s} \\ \hat{u} \\ \hat{v} \end{pmatrix} = \begin{pmatrix} \frac{3}{2}i\xi_2 & -i\xi_2 & i\xi_1 & 0 & 0 \\ -\frac{1}{8}i\xi_2 & \frac{3}{2}i\xi_2 & 0 & \frac{1}{4}i\xi_1 & -\frac{1}{4}i\xi_2 \\ \frac{1}{8}i\xi_1 & 0 & \frac{3}{2}i\xi_2 & \frac{1}{4}i\xi_2 & \frac{1}{4}i\xi_1 \\ \frac{\delta\xi_1\xi_2}{Re|\boldsymbol{\xi}|^2} & 0 & 0 & -\frac{1}{Re}|\boldsymbol{\xi}|^2 & 0 \\ -\frac{\delta\xi_1^2}{Re|\boldsymbol{\xi}|^2} & 0 & 0 & 0 & -\frac{1}{Re}|\boldsymbol{\xi}|^2 \end{pmatrix} \begin{pmatrix} \hat{\rho} \\ \hat{c} \\ \hat{s} \\ \hat{u} \\ \hat{v} \end{pmatrix} \tag{4.10}$$

In Figure 4.2, we plot the positive part of the spectral abscissa for the matrix on the right hand side of equation (4.10) for different values of Re and δ. We observe a wavelength selection mechanism which depends on Re and δ.

PROPOSITION 4.1. *Consider horizontal waves, i.e.* $\xi_2 = 0$. *For* $Re = 0$, *the coupled system describing the sedimentation of non-Brownian particles is linearly stable provided that the eigenvalue*

$$\lambda_0 = \sqrt{\frac{\delta}{4} - \frac{\xi_1^2}{8}}$$

is smaller than zero, otherwise it is unstable.

For $Re > 0$, *(*$Re \ll 1$*) the change of this eigenvalue can be expressed by an asymptotic expansion of the form*

$$\lambda = \sqrt{\frac{\delta}{4} - \frac{\xi_1^2}{8}} - (Re)\frac{\delta}{8\xi_1^2} + \dots. \tag{4.11}$$

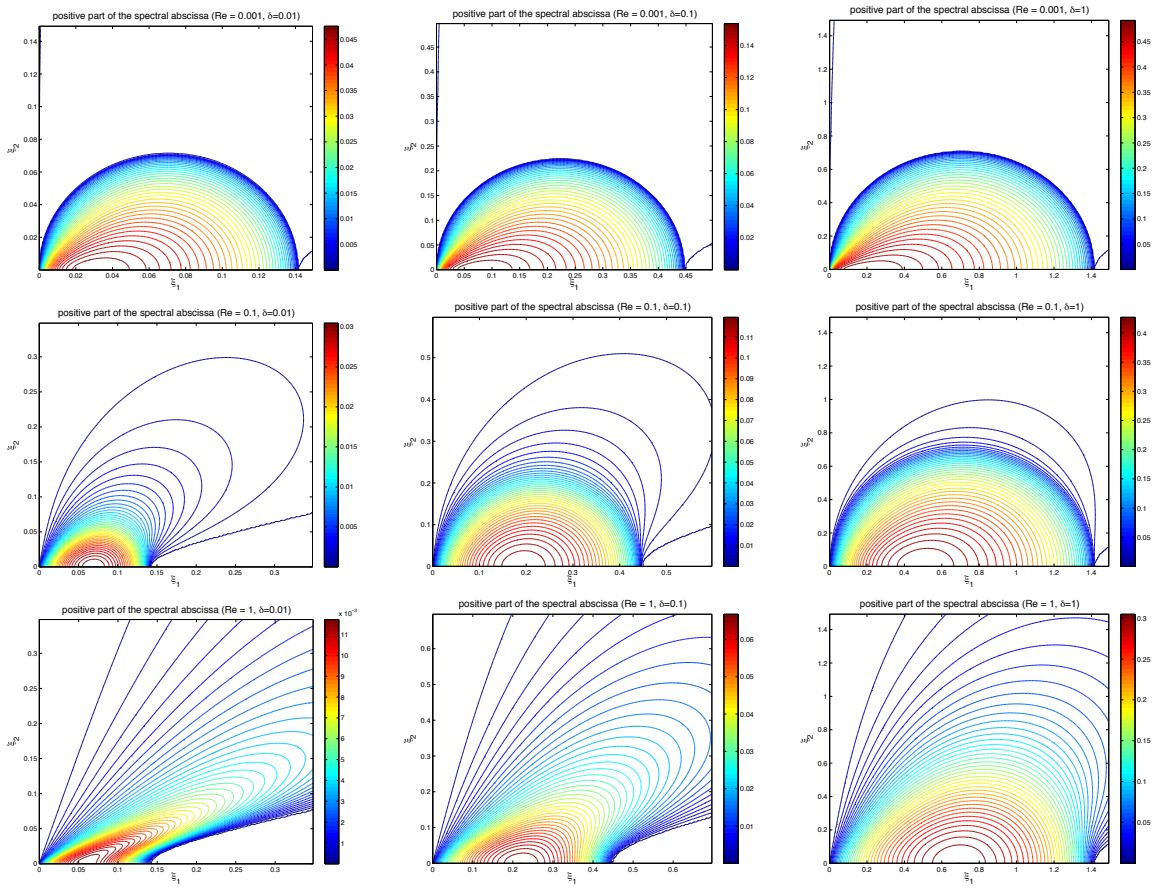

FIG. 4.2. *Positive part of spectral abscissa for the matrix arising in the linear stability analysis of the system modeling the sedimentation of non-Brownian particles in a flow with* $Re > 0$. *Different values of* Re *and* δ *are considered.*

The proof can be carried out in analogy to Proposition 3.1. Using the same notation, the eigenvalues of the matrix $A - BC^{-1}D$ are now

$$\{0, -\sqrt{\frac{\delta}{4} - \frac{\xi_1^2}{8}}, \sqrt{\frac{\delta}{4} - \frac{\xi_1^2}{8}}\}.$$

The eigenvector corresponding to the last eigenvalue (which we denote with λ_0) is

$$\boldsymbol{x} = \left(\frac{2\sqrt{2}\xi_1 i}{\sqrt{2\delta - \xi_1^2}}, 0, 1 \right)^T.$$

The left null space of the matrix

$$\begin{pmatrix} A - \lambda_0 I & B \\ D & C \end{pmatrix}$$

is the vector

$$\left(-\sqrt{4\delta - 2\xi_1^2}, 0, -4\xi_1 i, 0, 1 \right).$$

Using all these terms, one can carry out the calculation leading to (4.11).

For horizontal waves we now derive an approximative expression for the most unstable wavenumber as a function of the parameter values Re and δ. We rewrite the leading terms of (4.11) in the form

$$\begin{aligned}\lambda &= \frac{\sqrt{\delta}}{2}\sqrt{1-\frac{\xi_1^2}{2\delta}} - Re\frac{\delta}{8\xi_1^2} \\ &= \frac{\sqrt{\delta}}{2}\sqrt{1-x} - \frac{Re}{16}\frac{1}{x},\end{aligned}$$

with $x = \frac{\xi_1^2}{2\delta}$. For $x \ll 1$, we can use the approximation

$$\lambda \approx \frac{\sqrt{\delta}}{2}\left(1-\frac{x}{2}\right) - \frac{Re}{16}\frac{1}{x} = \tilde{\lambda}.$$

$\tilde{\lambda}$ attains a maximum for $x = \frac{1}{2}Re^{1/2}\delta^{-1/4}$, which corresponds to the most unstable wavenumber

$$\xi_1 = Re^{1/4}\delta^{3/8}. \tag{4.12}$$

In Figure 4.3 we show plots of the spectral abscissa for horizontal waves (solid line) and the approximation of the largest eigenvalue as calculated from (4.11) (plus symbols). For small values of Re (here we used $Re = 10^{-4}$ and $Re = 10^{-3}$) the expansion (4.11) is a good approximation of the spectral abscissa. The dashed line indicates the approximation of the most unstable wavenumber as calculated from (4.12).

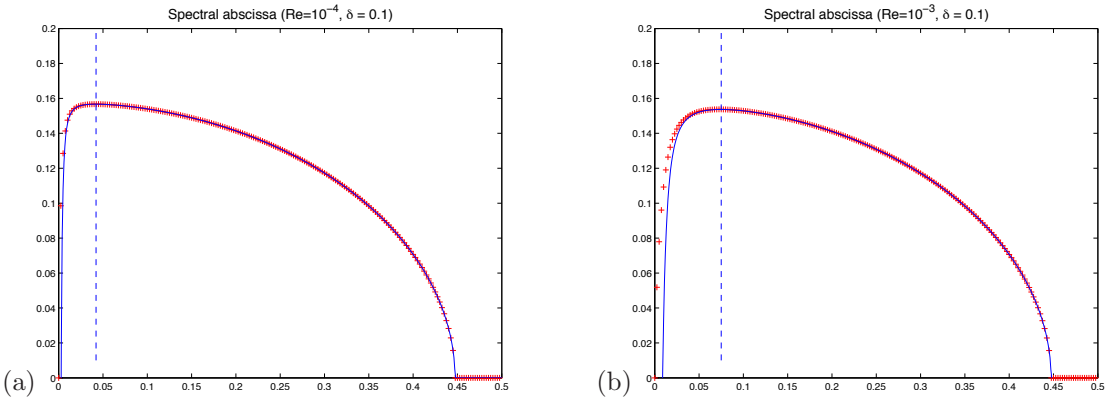

FIG. 4.3. *Positive part of spectral abscissa for horizontal wave over wavenumber (solid line), $\lambda(\xi_1)$ as calculated from (4.11) (plus symbol), most unstable wavenumber as approximated by (4.12) (dashed line); (a) $Re = 10^{-4}$, $\delta = 0.1$, (b) Re^{-3}, $\delta = 0.1$.*

Now we compare the predicted most unstable wavelength with experimental studies from [10]. The experiments where performed using glas rods with particle density $\rho_p = 2.25\frac{g}{cm^3}$, particle length $l_p = 0.108cm$ and diameter $d_p = 0.0102cm$. The particles are suspended in a fluid with fluid viscosity $\mu = 5.5\frac{g}{cms}$ and density $\rho_f = 1.07\frac{g}{cm^3}$. The particle volume fraction in the suspension is 0.48%. From those data we calculate the volume of a single particle $V_p = \pi\left(\frac{d_p}{2}\right)^2 l_p = 8.825\cdot 10^{-6}cm^3$, the mass of one particle $m_0 = \rho_p V_p = 1.98562\cdot 10^{-5}g$, the number density $\frac{N}{V} = 0.0048/V_p = 543.9103cm^{-3}$, and the translational friction coefficient $\zeta_\perp = \frac{4\pi\mu l_p}{\ln(l_p/d_p)} = 3.1632\frac{g}{s}$ (using the formula from [5, Section 8.3]). Our characteristic length and time scales are $X = 3.8655\cdot 10^{-8}cm = 3.5792\cdot 10^{-7}l_p$ and $T = 6.2773\cdot 10^{-6}s$. The nondimensional parameters can now be calculated and we obtain the values $Re = 4.6308\times 10^{-11}$ and $\delta = 4.6729\cdot 10^{-13}$. Via (4.12) the predicted most unstable wavenumber is $\xi_1 = 6.2017\cdot 10^{-8}$ which corresponds to a predicted selected wavelength of the size $\frac{X}{\xi_1} = 5.7713l_p$. This is in good qualitative agreement with experimental studies which show the formation of clusters with a typical width of the size of a few particle lengths, see [10, 11, 14]. An increase of the number of particles (within the

dilute regime) leads to an increase of the parameter δ and via (4.12) to a decrease of the predicted most unstable wavelength. In experimental studies such a dependence of the cluster width from the concentration of particles was also observed. Furthermore, the length of the particles as well as the aspect ration affect the most unstable wavelength.

Finally, we show numerical simulations for the nonlinear model

$$\partial_t f + \partial_\theta \left(v_x \cos^2\theta f \right) - \partial_x \left(\sin\theta \cos\theta f \right) = 0$$
$$\partial_t v - v_{xx} = \left(1 - \int_{S^1} f d\theta \right),$$

with initial values as specified in (3.39). We choose $L = 500$ and discretize the macroscopic domain $[0, L)$ with 8000 grid cells. The Smoluchowski equation is discretized using 100 grid cells. In Figure 4.4 we plot the density ρ and the result of the Fourier transformation of the data vs. wave number at time $t = 35$. The observed wavelength selection (with a wave number of about 0.7) is in good agreement with the prediction of the linear stability, compare with Figure 4.2 ($\delta = 1$, $Re = 1$).

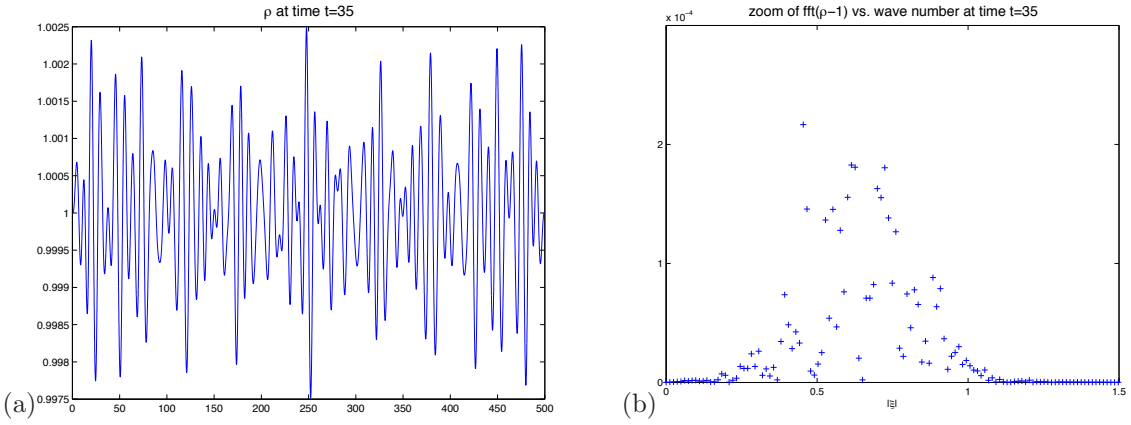

FIG. 4.4. *Simulations of the one-dimensional nonlinear model for $\delta = 1$ and $Re = 1$.*

5. The hyperbolic and diffusive scalings. Relation to the Keller-Segel model. In this section we derive the hyperbolic and diffusive limits for the system (2.27) with $Re = 0$. The limiting behavior in the hyperbolic scaling will be described by a Boussinesq type system. For certain flows the hyperbolic scaling produces a trivial behavior, and it is then natural to consider the diffusive scaling. Such a situation occurs for two-dimensional rectilinear flows of suspensions. We will show that the collective behavior in the diffusive limit is described by the Keller-Segel model

It is expedient to view the scaling limits from the perspective of the question of describing the aggregate behavior of a suspension starting from rest. The function

$$\rho(\boldsymbol{x}, t) = \int_{S^{d-1}} f(\boldsymbol{x}, t, \boldsymbol{n}) d\boldsymbol{n}$$

measures the density of rod-like particles. As discussed in the previous section, linear stability theory predicts an instability and a wavelength selection mechanism for modulations of ρ.

For such a problem it is natural to ask how the aggregate response of the system is described in long times. Our analysis of the diffusive scaling will show that it is described by the Keller-Segel model.

5.1. The hyperbolic limit. With the goal to derive equations describing the aggregate behavior of the suspension, we turn to calculate the hyperbolic and diffusive limits.

We first rescale the model (2.27) (with $Re = 0$) in the *hyperbolic scaling*,

$$\boldsymbol{x} = \frac{1}{\delta}\hat{\boldsymbol{x}},\ t = \frac{1}{\delta}\hat{t},\ \boldsymbol{u} = \hat{\boldsymbol{u}},\ p = \hat{p}.$$

The scaled equations (after dropping the hats) are

$$\begin{aligned} \delta\partial_t f + \delta \boldsymbol{u}\cdot\nabla_{\boldsymbol{x}} f - \delta D(\boldsymbol{n})\boldsymbol{e}_2\cdot\nabla_{\boldsymbol{x}} f + \delta\nabla_{\boldsymbol{n}}\cdot(P_{\boldsymbol{n}^\perp}\nabla_{\boldsymbol{x}}\boldsymbol{u}\boldsymbol{n} f) \\ = \Delta_{\boldsymbol{n}} f + \delta^2\gamma\nabla_{\boldsymbol{x}}\cdot D(\boldsymbol{n})\nabla_{\boldsymbol{x}} f \\ -\delta^2\Delta_{\boldsymbol{x}}\boldsymbol{u} + \delta\nabla_{\boldsymbol{x}} p - \delta^2\gamma\nabla_{\boldsymbol{x}}\cdot\sigma = -\delta\left(\int_{S^2} f d\boldsymbol{n}\right)\boldsymbol{e}_2 \\ \delta\nabla_{\boldsymbol{x}}\cdot\boldsymbol{u} = 0 \end{aligned} \tag{5.1}$$

where $D(\boldsymbol{n}) = I + \boldsymbol{n}\otimes\boldsymbol{n}$.

We introduce the ansatz

$$\begin{aligned} f &= \delta f_0 + \delta^2 f_1 + \dots \\ \boldsymbol{u} &= \boldsymbol{u}_0 + \delta\boldsymbol{u}_1 + \dots \\ p &= \delta p_0 + \delta^2 p_1 + \dots \end{aligned}$$

to the system (5.1) and obtain equations for the various orders of the expansion:

$$O(\delta) \qquad \Delta_{\boldsymbol{n}} f_0 = 0 \tag{5.2}$$

$$O(\delta^2) \qquad \partial_t f_0 + \boldsymbol{u}_0\cdot\nabla_{\boldsymbol{x}} f_0 - D(\boldsymbol{n})\boldsymbol{e}_2\cdot\nabla_{\boldsymbol{x}} f_0 + \nabla_{\boldsymbol{n}}\cdot(P_{\boldsymbol{n}^\perp}\nabla_{\boldsymbol{x}}\boldsymbol{u}_0\boldsymbol{n} f_0) = \Delta_{\boldsymbol{n}} f_1 \tag{5.3}$$

$$O(\delta^2) \qquad -\Delta_{\boldsymbol{x}}\boldsymbol{u}_0 + \nabla_{\boldsymbol{x}} p_0 = -\left(\int_{S^2} f_0 d\boldsymbol{n}\right)\boldsymbol{e}_2$$

$$O(\delta) \qquad \nabla_{\boldsymbol{x}}\cdot\boldsymbol{u}_0 = 0$$

It follows from (5.2) that f_0 is independent of $\boldsymbol{n}$ and thus

$$f_0(t,\boldsymbol{x},\boldsymbol{n}) = \frac{1}{4\pi}\int_{S^2} f_0 d\boldsymbol{n} = \frac{1}{4\pi}\rho_0(t,\boldsymbol{x})$$

Then integrating (5.3) over the sphere, we deduce that $\rho_0 = \int_{S^2} f_0 d\boldsymbol{n}$ and $\boldsymbol{u}_0$ satisfy the Boussinesq system

$$\begin{aligned} \partial_t\rho_0 + \nabla_{\boldsymbol{x}}\cdot\left(\boldsymbol{u}_0\rho_0 - \big(\frac{1}{4\pi}\int_{S^2} D(\boldsymbol{n})d\boldsymbol{n}\big)\boldsymbol{e}_2\rho_0\right) = 0 \\ -\Delta_{\boldsymbol{x}}\boldsymbol{u}_0 + \nabla_{\boldsymbol{x}} p_0 = -\rho_0\boldsymbol{e}_2 \\ \nabla_{\boldsymbol{x}}\cdot\boldsymbol{u}_0 = 0 \end{aligned} \tag{5.4}$$

5.2. The diffusive limit. Next, we consider rectilinear flows with a vertical velocity field obeying the ansatz

$$\boldsymbol{u}(t,x,z) = (0, v(t,x,z), 0)^T\ , \quad f = f(t,x,z)$$

and depending only on the horizontal variables. This restriction - to the two-dimensional case - is motivated by experimental observations of long clusters with higher particle density.

Indeed, for flows as above the hydrodynamic scale produces a trivial equation and one may consider the behavior in the diffusive scaling. We will show that in the diffusive scale the aggregate behavior of the system is described by the Keller-Segel system, which is known to provide a nonlinear concentration mechanism.

In the sequel we will monitor the quantities

$$\begin{aligned} f(t,\boldsymbol{x},\boldsymbol{n}) &= \hat{f}(t,\boldsymbol{x} + t\boldsymbol{e}_2\frac{1}{4\pi}\int_{S^2} D(\boldsymbol{n})d\boldsymbol{n},\boldsymbol{n}) \\ \boldsymbol{u}(t,\boldsymbol{x}) &= \hat{\boldsymbol{u}}(t,\boldsymbol{x} + t\boldsymbol{e}_2\frac{1}{4\pi}\int_{S^2} D(\boldsymbol{n})d\boldsymbol{n}) \end{aligned} \tag{5.5}$$

Then $\hat{f}$ and $\hat{\boldsymbol{u}}$ satisfy

$$\begin{aligned}\partial_t \hat{f} + \hat{\boldsymbol{u}} \cdot \nabla_{\boldsymbol{x}} \hat{f} - \left(D(\boldsymbol{n}) - \frac{1}{4\pi} \int_{S^2} D(\boldsymbol{n}) d\boldsymbol{n} \right) \boldsymbol{e}_2 \cdot \nabla_{\boldsymbol{x}} \hat{f} \\ + \nabla_{\boldsymbol{n}} \cdot \left(P_{\boldsymbol{n}^\perp} \nabla_{\boldsymbol{x}} \hat{\boldsymbol{u}} \boldsymbol{n} \hat{f} \right) = \Delta_{\boldsymbol{n}} \hat{f} + \gamma \nabla_{\boldsymbol{x}} \cdot D(\boldsymbol{n}) \nabla_{\boldsymbol{x}} \hat{f}. \qquad (5.6) \\ -\Delta_{\boldsymbol{x}} \hat{\boldsymbol{u}} + \nabla_{\boldsymbol{x}} \hat{p} - \gamma \delta \nabla_{\boldsymbol{x}} \cdot \hat{\sigma} = -\delta \left(\int_{S^2} \hat{f} d\boldsymbol{n} \right) \boldsymbol{e}_2\end{aligned}$$

We rescale the model using the *diffusive scaling*, i.e.

$$\boldsymbol{x} = \frac{1}{\delta} \hat{\boldsymbol{x}}, \ t = \frac{1}{\delta^2} \hat{t}, \ \boldsymbol{u} = \hat{\boldsymbol{u}}, \ p = \hat{p}. \qquad (5.7)$$

The scaled equations (dropping the hats) have the form

$$\begin{aligned}\delta^2 \partial_t f + \delta \boldsymbol{u} \cdot \nabla_{\boldsymbol{x}} f - \delta \left(D(\boldsymbol{n}) - \frac{1}{4\pi} \int_{S^2} D(\boldsymbol{n}) d\boldsymbol{n} \right) \boldsymbol{e}_2 \cdot \nabla_{\boldsymbol{x}} f \\ + \delta \nabla_{\boldsymbol{n}} \cdot (P_{\boldsymbol{n}^\perp} \nabla_{\boldsymbol{x}} \boldsymbol{u} \boldsymbol{n} f) = \Delta_{\boldsymbol{n}} f + \delta^2 \gamma \nabla_{\boldsymbol{x}} \cdot D(\boldsymbol{n}) \nabla_{\boldsymbol{x}} f \\ -\delta^2 \Delta_{\boldsymbol{x}} \boldsymbol{u} + \delta \nabla_{\boldsymbol{x}} p - \delta^2 \gamma \nabla_{\boldsymbol{x}} \cdot \sigma = -\delta \left(\int_{S^2} f d\boldsymbol{n} \right) \boldsymbol{e}_2 \\ \nabla_{\boldsymbol{x}} \cdot \boldsymbol{u} = 0\end{aligned}$$

We introduce the ansatz

$$\begin{aligned} f(t, x, z, \boldsymbol{n}) &= \delta f_0 + \delta^2 f_1 + \dots \\ \boldsymbol{u}(t, x, z) &= \boldsymbol{u}_0 + \delta \boldsymbol{u}_1 + \dots = \begin{pmatrix} 0 \\ v_0 \\ 0 \end{pmatrix} + \delta \begin{pmatrix} 0 \\ v_1 \\ 0 \end{pmatrix} + \dots \\ p &= \delta p_0 + \delta^2 p_1 + \dots \end{aligned}$$

to the above system and collect the terms of the same order, thus arriving at

$$O(\delta) \qquad \Delta_{\boldsymbol{n}} f_0 = 0 \qquad (5.8)$$

$$O(\delta^2) \qquad -\left(D(\boldsymbol{n}) - \frac{1}{4\pi} \int_{S^2} D(\boldsymbol{n}) d\boldsymbol{n} \right) \boldsymbol{e}_2 \cdot \nabla_{\boldsymbol{x}} f_0 + \nabla_{\boldsymbol{n}} \cdot (P_{\boldsymbol{n}^\perp} \nabla_{\boldsymbol{x}} \boldsymbol{u}_0 \boldsymbol{n} f_0) = \Delta_{\boldsymbol{n}} f_1 \qquad (5.9)$$

$$\begin{aligned} O(\delta^3) \qquad & \partial_t f_0 - \left(D(\boldsymbol{n}) - \frac{1}{4\pi} \int_{S^2} D(\boldsymbol{n}) d\boldsymbol{n} \right) \boldsymbol{e}_2 \cdot \nabla_{\boldsymbol{x}} f_1 \left(P_{\boldsymbol{n}^\perp} \left(\nabla_{\boldsymbol{x}} \boldsymbol{u}_1 \boldsymbol{n} f_0 + \nabla_{\boldsymbol{x}} \boldsymbol{u}_0 \boldsymbol{n} f_1 \right) \right) \\ & = \Delta_{\boldsymbol{n}} f_2 + \gamma \nabla_{\boldsymbol{x}} \cdot D(\boldsymbol{n}) \nabla_{\boldsymbol{x}} f_0 \qquad (5.10) \end{aligned}$$

Here, we used the fact that due to the form of the ansatz all terms of the type $\boldsymbol{u}_i \cdot (\nabla_{\boldsymbol{x}} f)_j = 0$ vanish. The same procedure applied to the Stokes system yields

$$\begin{aligned} O(\delta^2) \qquad & -\Delta_{\boldsymbol{x}} \boldsymbol{u}_0 + \nabla_{\boldsymbol{x}} p_0 = -\left(\int_{S^2} f_0 d\boldsymbol{n} \right) \boldsymbol{e}_2 \\ O(\delta) \qquad & \nabla_{\boldsymbol{x}} \cdot \boldsymbol{u}_0 = 0 \end{aligned}$$

Equation (5.8) implies that f_0 is independent on $\boldsymbol{n}$, that is

$$f_0 = \frac{1}{4\pi} \int_{S^2} f_0 d\boldsymbol{n} = \frac{1}{4\pi} \rho_0(t, x, z)$$

Next, integration of (5.10) over the sphere gives that ρ_0 satisfies

$$\partial_t \rho_0 = \nabla_{\boldsymbol{x}} \cdot \underbrace{\int_{S^2} \left(D(\boldsymbol{n}) - \frac{1}{4\pi} \int_{S^2} D(\boldsymbol{n}) d\boldsymbol{n} \right) \boldsymbol{e}_2 f_1 \, d\boldsymbol{n}}_{=:I_1} + \gamma \nabla_{\boldsymbol{x}} \cdot \underbrace{\frac{1}{4\pi} \int_{S^2} D(\boldsymbol{n}) d\boldsymbol{n}}_{=:I_2} \nabla_{\boldsymbol{x}} \rho_0 \qquad (5.11)$$

where the terms I_1 and I_2 are computed in terms of f_1 solving (5.9) for $f_0 = \frac{1}{4\pi}\rho_0$.

It remains to compute the terms I_1 and I_2. Observe now that we have the identities:

$$\begin{aligned}
\int_{S^2} (\boldsymbol{n}\otimes\boldsymbol{n} - \frac{1}{3}I)d\boldsymbol{n} &\overset{(B.4)}{=} -\frac{1}{6}\int_{S^2} \triangle_{\boldsymbol{n}}(\boldsymbol{n}\otimes\boldsymbol{n} - \frac{1}{3}I)d\boldsymbol{n} = 0\\
I_2 := \frac{1}{4\pi}\int_{S^2} D(\boldsymbol{n})d\boldsymbol{n} &= \frac{1}{4\pi}\int_{S^2}(\boldsymbol{n}\otimes\boldsymbol{n} + I)d\boldsymbol{n} = \frac{4}{3}I \qquad (5.12)\\
D(\boldsymbol{n}) - \frac{1}{4\pi}\int_{S^2} D(\boldsymbol{n})d\boldsymbol{n} &= \boldsymbol{n}\otimes\boldsymbol{n} - \frac{1}{3}I
\end{aligned}$$

These, in conjunction with (5.8), (5.9) and (B.7), imply that f_1 satisfies

$$\begin{aligned}
\Delta_{\boldsymbol{n}} f_1 &= -\big(D(\boldsymbol{n}) - \frac{1}{4\pi}\int_{S^2} D(\boldsymbol{n})d\boldsymbol{n}\big)\boldsymbol{e}_2\cdot\frac{1}{4\pi}\nabla_{\boldsymbol{x}}\rho_0 + \frac{1}{4\pi}\nabla_{\boldsymbol{n}}\cdot\left(P_{\boldsymbol{n}^\perp}\nabla_{\boldsymbol{x}}\boldsymbol{u}_0\boldsymbol{n}\right)\rho_0\\
&= -\big(\boldsymbol{n}\otimes\boldsymbol{n} - \frac{1}{3}I\big)\boldsymbol{e}_2\cdot\frac{1}{4\pi}\nabla_{\boldsymbol{x}}\rho_0 - \frac{3}{4\pi}\rho_0(\boldsymbol{n}\cdot\nabla_{\boldsymbol{x}}\boldsymbol{u}_0\boldsymbol{n}) \qquad (5.13)
\end{aligned}$$

Next, we compute I_1

$$\begin{aligned}
I_1 &:= \int_{S^2}\left(D(\boldsymbol{n}) - \frac{1}{4\pi}\int_{S^2} D(\boldsymbol{n})d\boldsymbol{n}\right)\boldsymbol{e}_2 f_1\, d\boldsymbol{n}\\
&= \int_{S^2}\big(\boldsymbol{n}\otimes\boldsymbol{n} - \frac{1}{3}I\big)\boldsymbol{e}_2 f_1 d\boldsymbol{n}\\
&\overset{(B.4)}{=} -\frac{1}{6}\int_{S^2}\triangle_{\boldsymbol{n}}\big(\boldsymbol{n}\otimes\boldsymbol{n} - \frac{1}{3}I\big)\boldsymbol{e}_2 f_1 d\boldsymbol{n}\\
&\overset{(5.13)}{=} \frac{1}{24\pi}\int_{S^2}\big(\boldsymbol{n}\otimes\boldsymbol{n} - \frac{1}{3}I\big)\boldsymbol{e}_2\Big[\big(\boldsymbol{n}\otimes\boldsymbol{n} - \frac{1}{3}I\big)\boldsymbol{e}_2\cdot\nabla_{\boldsymbol{x}}\rho_0 + 3\rho_0(\boldsymbol{n}\cdot\nabla_{\boldsymbol{x}}\boldsymbol{u}_0\boldsymbol{n})\Big]d\boldsymbol{n}\\
&= \frac{1}{24\pi}\int_{S^2}\begin{pmatrix} n_1 n_2\\ n_2^2 - \frac{1}{3}\\ n_2 n_3\end{pmatrix}\Big[(3\rho_0 v_{0x} + \rho_{0x})n_1 n_2 + (3\rho_0 v_{0z} + \rho_{0z})n_2 n_3\Big]d\boldsymbol{n}
\end{aligned}$$

Observe that, due to symmetry considerations, the integrals

$$\begin{aligned}
\int_{S^2} n_1 n_2^3 - \frac{1}{3}n_1 n_2 d\boldsymbol{n} = 0\\
\int_{S^2} n_2^3 n_3 - \frac{1}{3}n_2 n_3 d\boldsymbol{n} = 0\\
\int_{S^2} n_1 n_2^2 n_3 d\boldsymbol{n} = = 0,
\end{aligned}$$

while the remaining integrals are computed via spherical coordinates

$$\begin{aligned}
\int_{S^2} n_1^2 n_2^2 d\boldsymbol{n} = \int_0^\pi \sin^5\theta\, d\theta\int_0^{2\pi}\sin^2\varphi\cos^2\varphi d\varphi = \frac{4\pi}{15}\\
\int_{S^2} n_2^2 n_3^2 d\boldsymbol{n} = \int_0^\pi \sin^3\theta\cos^2\theta\, d\theta\int_0^{2\pi}\sin^2\varphi d\varphi = \frac{4\pi}{15}.
\end{aligned}$$

We conclude that

$$I_1 = \frac{1}{90}\left(3\rho_0 v_{0x} + \rho_{0x}\,,\ 0\ ,3\rho_0 v_{0z} + \rho_{0z}\right)^T$$

and that ρ_0 satisfies the equation

$$\begin{aligned}
\partial_t\rho_0 &= \frac{1}{30}\left(\partial_x\left(\frac{1}{3}\rho_{0x} + \rho_0 v_{0x}\right) + \partial_z\left(\frac{1}{3}\rho_{0z} + \rho_0 v_{0z}\right)\right) + \gamma\frac{4}{3}\Delta_{(x,z)}\rho_0\\
&= \frac{1}{30}\nabla_{(x,z)}\cdot\left(\rho_0\nabla_{(x,z)}v_0\right) + \frac{1}{3}\left(4\gamma + \frac{1}{30}\right)\triangle_{(x,z)}\rho_0
\end{aligned}$$

We summarize the result:

PROPOSITION 5.1. *Let $f(t,x,z,\boldsymbol{n})$, $\boldsymbol{u}(t,x,z) = (0, v(t,x,z), 0)$ be a solution of (5.6). In the diffusive scaling (5.7) the leading order terms $f_0 = \frac{1}{4\pi}\rho_0(t,x,z)$ and $v_0(t,x,z)$ satisfy the Keller-Segel model*

$$\begin{aligned} \partial_t \rho_0 &= \frac{1}{30}\nabla_{(x,z)} \cdot \big(\rho_0 \nabla_{(x,z)} v_0\big) + \frac{1}{3}\big(4\gamma + \frac{1}{30}\big)\triangle_{(x,z)}\rho_0 \\ \Delta_{(x,z)} v_0 &= \rho_0. \end{aligned} \tag{5.14}$$

Conclusions. We present a kinetic model for the sedimentation of dilute suspensions of rod-like Brownian particles in low Reynolds number flow. This model describes concentration and the formation of clusters with higher particle density. Such phenomena have previously been observed in experimental and numerical studies of non-Brownian particles.

By restricting considerations to second moments, we derive a linear model and study the linear stability. We show that a non-zero Reynolds number leads to a wavelength selection mechanism. This indicates that inertial effects (which have often been excluded in related mathematical models) can influence the pattern formation on the macroscopic scale.

Furthermore, we show that at large times the macroscopic behavior of the system can be described by a Keller-Segel equation.

Appendix A. Linear moment closure. Here we give the details on the derivation of the two-dimensional linear moment closure system used in Section 3.

Using the relations

$$\begin{aligned} \sin^2\theta &= \frac{1}{2}\left(1 - \cos(2\theta)\right), \quad \cos^2\theta = \frac{1}{2}\left(1 + \cos(2\theta)\right) \\ D(\boldsymbol{n})\boldsymbol{e}_2 \nabla_{\boldsymbol{x}} f &= \frac{1}{2}\left(\partial_x f \sin(2\theta) + \partial_y f\left(3 - \cos(2\theta)\right)\right) \\ \nabla_{\boldsymbol{n}} \cdot (P_{\boldsymbol{n}^\perp} \nabla_{\boldsymbol{x}} \boldsymbol{u}\boldsymbol{n}) &= \partial_\theta \left(\boldsymbol{n}^\perp \cdot \nabla_{\boldsymbol{x}} \boldsymbol{u}\boldsymbol{n}\right) \\ &= \partial_\theta \left(\begin{pmatrix} -\sin\theta \\ \cos\theta \end{pmatrix} \cdot \nabla_{\boldsymbol{x}} \boldsymbol{u} \begin{pmatrix} \cos\theta \\ \sin\theta \end{pmatrix} \right) \\ &= (v_y - u_x)\cos(2\theta) - (u_y + v_x)\sin(2\theta) \\ \nabla_{\boldsymbol{x}} \cdot D(\boldsymbol{n}) \nabla_{\boldsymbol{x}} f &= \frac{1}{2}\left(3 + \cos(2\theta)\right)\partial_{xx} f + \sin(2\theta)\partial_{xy} f + \frac{1}{2}\left(3 - \cos(2\theta)\right)\partial_{yy} f \end{aligned}$$

we rewrite the linearized Smoluchowski equation (3.1) into the form

$$\begin{aligned} \partial_t f = & \underbrace{\frac{1}{2}\left(\sin(2\theta)\,\partial_x f + \left(3 - \cos(2\theta)\right)\partial_y f\right)}_{(I)} \\ & + \underbrace{\frac{1}{2\pi}(u_x - v_y)\cos(2\theta) + \frac{1}{2\pi}(u_y + v_x)\sin(2\theta)}_{(II)} \\ & + \underbrace{\partial_\theta^2 f}_{(III)} + \underbrace{\gamma\left(\frac{1}{2}(3 + \cos(2\theta))\partial_{xx} f + \sin(2\theta)\partial_{xy} f + \frac{1}{2}(3 - \cos(2\theta))\partial_{yy} f\right)}_{(IV)}. \end{aligned} \tag{A.1}$$

We consider a closure at the level of second moments

$$\rho(\boldsymbol{x},t) := \int_0^{2\pi} f(\boldsymbol{x},\theta,t)\,d\theta, c(\boldsymbol{x},t) := \frac{1}{2}\int_0^{2\pi} \cos(2\theta) f\,d\theta, s(\boldsymbol{x},t) := \frac{1}{2}\int_0^{2\pi} \sin(2\theta) f\,d\theta \tag{A.2}$$

and derive evolution equations for ρ, c and s.

Evolution equation for ρ:. The evolution of ρ can be expressed by

$$\partial_t \rho = \int_0^{2\pi} \partial_t f \, d\theta.$$

We replace $\partial_t f$ by the terms on the right hand side of (A.1). Note that there is no contribution from (II) and (III).

Contribution from (I):

$$\int_0^{2\pi} \frac{1}{2} \left(\sin(2\theta)\partial_x f + (3 - \cos(2\theta))\partial_y f \right) \, d\theta = s_x + \frac{3}{2}\rho_y - c_y$$

Contribution from (IV):

$$\begin{aligned} &\int_0^{2\pi} \gamma \left(\frac{3 + \cos(2\theta)}{2} \partial_{xx} f + \sin(2\theta)\partial_{xy} f + \frac{3 - \cos(2\theta)}{2} \partial_{yy} f \right) \, d\theta \\ &= \gamma \left(\frac{3}{2}(\rho_{xx} + \rho_{yy}) + 2s_{xy} + c_{xx} - c_{yy} \right) \end{aligned}$$

Thus we obtain

$$\partial_t \rho = \frac{3}{2}\rho_y - c_y + s_x + \gamma \left(\frac{3}{2}(\rho_{xx} + \rho_{yy}) + 2s_{xy} + c_{xx} - c_{yy} \right) \tag{A.3}$$

Evolution equation for c:.

$$\partial_t c = \frac{1}{2} \int_0^{2\pi} \cos(2\theta) \partial_t f \, d\theta.$$

Contribution from (I):

$$\begin{aligned} &\frac{1}{4} \int_0^{2\pi} \cos(2\theta) \left(\sin(2\theta)\partial_x f + (3 - \cos(2\theta))\partial_y f \right) \, d\theta \\ &= \frac{1}{2} \int_0^{2\pi} \sin(4\theta)\partial_x f \, d\theta + \frac{3}{2} c_y - \frac{1}{4} \int_0^{2\pi} \underbrace{\cos^2(2\theta)}_{= \frac{1}{2}(1 + \cos(4\theta))} \partial_y f \, d\theta \\ &\doteq \frac{3}{2} c_y - \frac{1}{8} \rho_y \end{aligned}$$

In this approximation (notation $\doteq$) we neglect terms that involve integrals of the form $\int_0^{2\pi} \sin(4\theta) q \, d\theta$ and $\int_0^{2\pi} \cos(4\theta) q \, d\theta$, respectively.

Contribution from (II):

$$\begin{aligned} &\frac{1}{2} \frac{1}{2\pi} \int_0^{2\pi} \cos(2\theta) \left[(u_x - v_y)\cos(2\theta) + (u_y + v_x)\sin(2\theta) \right] \, d\theta \\ &= \frac{1}{2} \frac{1}{2\pi} \left(\int_0^{2\pi} (u_x - v_y) \underbrace{\cos^2(2\theta)}_{= \frac{1}{2}(1 + \cos(4\theta))} \, d\theta + \int_0^{2\pi} (u_y + v_x) \frac{1}{2} \sin(4\theta) \, d\theta \right) \\ &\doteq \frac{1}{4}(u_x - v_y) \end{aligned}$$

Contribution from (III):

$$\begin{aligned} \frac{1}{2} \int_0^{2\pi} \cos(2\theta) \left(\partial_\theta^2 f \right) \, d\theta &= \frac{1}{2} \int_0^{2\pi} 2\sin(2\theta)\partial_\theta f \, d\theta \\ &= -\int_0^{2\pi} 2\cos(2\theta) f \, d\theta \\ &= -4c \end{aligned}$$

Contribution from (IV):

$$\begin{aligned}
&\frac{1}{2}\gamma\int_0^{2\pi}\cos(2\theta)\left[\frac{3+\cos(2\theta)}{2}\partial_{xx}f+\sin(2\theta)\partial_{xy}f+\frac{3-\cos(2\theta)}{2}\partial_{yy}f\right]d\theta\\
&=\gamma\Big[\frac{3}{2}c_{xx}+\frac{1}{4}\int_0^{2\pi}\underbrace{\cos^2(2\theta)}_{=\frac{1}{2}(1+\cos(4\theta))}\partial_{xx}f\,d\theta+\frac{1}{4}\int_0^{2\pi}\sin(4\theta)\partial_{xy}f\,d\theta+\frac{3}{2}c_{yy}\\
&\qquad\qquad-\frac{1}{4}\int_0^{2\pi}\cos^2(2\theta)\partial_{yy}f\,d\theta\Big]\\
&\doteq\gamma\left(\frac{3}{2}\left(c_{xx}+c_{yy}\right)+\frac{1}{8}\left(\rho_{xx}-\rho_{yy}\right)\right)
\end{aligned}$$

We obtain:

$$\partial_t c=-\frac{1}{8}\rho_y+\frac{3}{2}c_y+\frac{1}{4}(u_x-v_y)-4c+\gamma\Big(\frac{3}{2}\left(c_{xx}+c_{yy}\right)+\frac{1}{8}\left(\rho_{xx}-\rho_{yy}\right)\Big) \tag{A.4}$$

Evolution equation for s:.

$$\partial_t s=\frac{1}{2}\int_0^{2\pi}\sin(2\theta)\partial_t f\,d\theta.$$

Contribution from (I):

$$\begin{aligned}
&\frac{1}{4}\int_0^{2\pi}\sin(2\theta)\left[\sin(2\theta)\partial_x f+(3-\cos(2\theta))\partial_y f\right]d\theta\\
&=\frac{1}{4}\int_0^{2\pi}\underbrace{\sin^2(2\theta)}_{=\frac{1}{2}(1-\cos(4\theta))}\partial_x f\,d\theta+\frac{3}{2}s_y-\frac{1}{8}\int_0^{2\pi}\sin(4\theta)\partial_y f\,d\theta\\
&\doteq\frac{1}{8}\rho_x+\frac{3}{2}s_y
\end{aligned}$$

Contribution from (II):

$$\begin{aligned}
&\frac{1}{2}\frac{1}{2\pi}\int_0^{2\pi}\sin(2\theta)\left[(u_x-v_y)\cos(2\theta)+(u_y+v_x)\sin(2\theta)\right]d\theta\\
&=\frac{1}{4}\frac{1}{2\pi}(u_x-v_y)\int_0^{2\pi}\sin(4\theta)\,d\theta+\frac{1}{2}\frac{1}{2\pi}(u_y+v_x)\int_0^{2\pi}\sin^2(2\theta)\,d\theta\\
&\doteq\frac{1}{4}(u_y+v_x)
\end{aligned}$$

Contribution from (III):

$$\begin{aligned}
\frac{1}{2}\int_0^{2\pi}\sin(2\theta)(\partial_\theta^2 h)\,d\theta&=-\int_0^{2\pi}\cos(2\theta)\partial_\theta f\,d\theta\\
&=-2\int_0^{2\pi}\sin(2\theta)f\,d\theta\\
&=-4s
\end{aligned}$$

Contribution from (IV):

$$\begin{aligned}
&\frac{1}{2}\gamma\int_0^{2\pi}\sin(2\theta)\left[\frac{1}{2}(3+\cos(2\theta))\partial_{xx}f+\sin(2\theta)\partial_{xy}f+\frac{1}{2}(3-\cos(2\theta))\partial_{yy}f\right]d\theta\\
&\doteq\gamma\left[\frac{3}{2}s_{xx}+\frac{1}{2}\int_0^{2\pi}\sin^2(2\theta)\partial_{xy}f\,d\theta+\frac{3}{2}s_{yy}\right]\\
&\doteq\gamma\left(\frac{3}{2}(s_{xx}+s_{yy})+\frac{1}{4}\rho_{xy}\right)
\end{aligned}$$

We obtain

$$\partial_t s = \frac{1}{8}\rho_x + \frac{3}{2}s_y + \frac{1}{4}(u_y + v_x) - 4s + \gamma\left(\frac{1}{4}\rho_{xy} + \frac{3}{2}(s_{xx} + s_{yy})\right) \tag{A.5}$$

Appendix B. Properties of the differential operators in spherical coordinates.

The operator $\nabla_{\boldsymbol{n}}$ satisfies certain elementary properties that are extensively used in this article: Let $\boldsymbol{F}$ be a vector-valued function and f, g be scalar-valued functions, then

$$\int_{S^2}(\nabla_{\boldsymbol{n}}\cdot\boldsymbol{F})f\,d\boldsymbol{n} = -\int_{S^2}\boldsymbol{F}\cdot(\nabla_{\boldsymbol{n}}f - 2\boldsymbol{n}f)d\boldsymbol{n} \tag{B.1}$$

$$\int_{S^2}(\nabla_{\boldsymbol{n}}\cdot\nabla_{\boldsymbol{n}}f)g\,d\boldsymbol{n} = \int_{S^2}(\nabla_{\boldsymbol{n}}\cdot\nabla_{\boldsymbol{n}}g)f\,d\boldsymbol{n} \tag{B.2}$$

$$\int_{S^2}\boldsymbol{n}\otimes\nabla_{\boldsymbol{n}}f\,d\boldsymbol{n} = \int_{S^2}\nabla_{\boldsymbol{n}}f\otimes\boldsymbol{n}\,d\boldsymbol{n} = \int_{S^2}(3\boldsymbol{n}\otimes\boldsymbol{n} - \mathrm{id})f\,d\boldsymbol{n} \tag{B.3}$$

The components of the tensor $3\boldsymbol{n}\otimes\boldsymbol{n} - \mathrm{id}$ are the surface spherical harmonics of order 2. That is they are harmonic polynomials on $\mathbb{R}^3$ of order 2, restricted to S^2. The surface spherical harmonics are eigenfunctions of the Laplacian on S^2 with corresponding eigenvalue $-\ell(\ell+1)$, where ℓ is the order [1, App. E]. Hence

$$\triangle_{\boldsymbol{n}}(3\,n_i\,n_j - \delta_{ij}) \;=\; -6\,(3\,n_i\,n_j - \delta_{ij}). \tag{B.4}$$

It is convenient to use spherical coordinates in proving such formulas, see [1, App. A.6 and E.6]. A point P with Cartesian coordinates (n_x, n_y, n_z) is expressed in spherical coordinates via

$$n_x = r\sin\theta\,\cos\varphi\,,\; n_y = r\sin\theta\,\sin\varphi\,,\; n_z = r\cos\theta$$

where $0 < \theta < \pi$, $0 \le \varphi < 2\pi$. Let $\boldsymbol{e}_r$, $\boldsymbol{e}_\theta$, $\boldsymbol{e}_\varphi$ be the orthonormal coordinate system associated to spherical coordinates and attached at P. It satisfies the derivative formulas

$$\begin{array}{lll}
\frac{\partial\boldsymbol{e}_r}{\partial r} = 0\,, & \frac{\partial\boldsymbol{e}_r}{\partial\theta} = \boldsymbol{e}_\theta\,, & \frac{\partial\boldsymbol{e}_r}{\partial\varphi} = \boldsymbol{e}_\varphi\,\sin\theta\,,\\
\frac{\partial\boldsymbol{e}_\theta}{\partial r} = 0\,, & \frac{\partial\boldsymbol{e}_\theta}{\partial\theta} = -\boldsymbol{e}_r\,, & \frac{\partial\boldsymbol{e}_\theta}{\partial\varphi} = \boldsymbol{e}_\varphi\,\cos\theta\,,\\
\frac{\partial\boldsymbol{e}_\varphi}{\partial r} = 0\,, & \frac{\partial\boldsymbol{e}_\varphi}{\partial\theta} = 0\,, & \frac{\partial\boldsymbol{e}_\varphi}{\partial\varphi} = -\boldsymbol{e}_r\,\sin\theta - \boldsymbol{e}_\theta\,\cos\theta\,.
\end{array} \tag{B.5}$$

We visualize the sphere S^2 as embedded in the Euclidean space. The surface gradient $\nabla_{\boldsymbol{n}}$ is related to the (ambient) gradient operator ∇ through

$$\nabla_{\boldsymbol{n}} = r(\mathrm{id} - \boldsymbol{n}\otimes\boldsymbol{n})\cdot\nabla = \boldsymbol{e}_\theta\frac{\partial}{\partial\theta} + \boldsymbol{e}_\varphi\frac{1}{\sin\theta}\frac{\partial}{\partial\varphi}$$

and, for a scalar-valued function f, the surface gradient and the Laplace-Beltrami operator are given respectively by

$$\nabla_{\boldsymbol{n}}f = \boldsymbol{e}_\theta\frac{\partial f}{\partial\theta} + \boldsymbol{e}_\varphi\frac{1}{\sin\theta}\frac{\partial f}{\partial\varphi}$$

$$\triangle_{\boldsymbol{n}}f = \nabla_{\boldsymbol{n}}\cdot\nabla_{\boldsymbol{n}}f = \frac{1}{\sin\theta}\frac{\partial}{\partial\theta}\left(\sin\theta\frac{\partial f}{\partial\theta}\right) + \frac{1}{\sin^2\theta}\frac{\partial^2 f}{\partial\varphi^2}$$

The divergence of a vector-valued function $\boldsymbol{F} = F_r\boldsymbol{e}_r + F_\theta\boldsymbol{e}_\theta + F_\varphi\boldsymbol{e}_\varphi$ has the form

$$\begin{aligned}
\nabla_{\boldsymbol{n}}\cdot\boldsymbol{F} &= \left(\boldsymbol{e}_\theta\frac{\partial}{\partial\theta} + \boldsymbol{e}_\varphi\frac{1}{\sin\theta}\frac{\partial}{\partial\varphi}\right)\cdot\left(\boldsymbol{F}_r\boldsymbol{e}_r + F_\theta\boldsymbol{e}_\theta + F_\varphi\boldsymbol{e}_\varphi\right)\\
&\overset{(B.5)}{=} \frac{1}{\sin\theta}\frac{\partial}{\partial\theta}\left(\sin\theta F_\theta\right) + \frac{1}{\sin\theta}\frac{\partial F_\varphi}{\partial\varphi} + 2F_r
\end{aligned}$$

It is now easy to compute (B.1)-(B.3). Observe that

$$\begin{aligned}\int_{S^2}(\nabla_{\boldsymbol{n}}\cdot\boldsymbol{F})f\,d\boldsymbol{n} &= \iint\left(\frac{1}{\sin\theta}\frac{\partial}{\partial\theta}\left(\sin\theta F_\theta\right)+\frac{1}{\sin\theta}\frac{\partial F_\varphi}{\partial\varphi}+2F_r\right)f\sin\theta\,d\theta d\varphi\\ &= -\iint\left(-2F_r f+F_\theta\frac{\partial f}{\partial\theta}+\frac{1}{\sin\theta}F_\varphi\frac{\partial f}{\partial\varphi}\right)\sin\theta\,d\theta d\varphi\\ &= -\int_{S^2}\boldsymbol{F}\cdot(\nabla_{\boldsymbol{n}}f-2\boldsymbol{n}f)d\boldsymbol{n}\end{aligned}$$

which gives (B.1), and (B.2) follows by applying (B.1) twice:

$$\begin{aligned}\int_{S^2}(\nabla_{\boldsymbol{n}}\cdot\nabla_{\boldsymbol{n}}f)g\,d\boldsymbol{n} &= -\int_{S^2}\nabla_{\boldsymbol{n}}f\cdot\left(\nabla_{\boldsymbol{n}}g-2\boldsymbol{n}g\right)d\boldsymbol{n}\\ &= \int_{S^2}f(\nabla_{\boldsymbol{n}}\cdot\nabla_{\boldsymbol{n}}g)d\boldsymbol{n}\,.\end{aligned}$$

Using integration by parts, we obtain the chain of identities

$$\begin{aligned}\int_{S^2}\boldsymbol{n}\otimes\nabla_{\boldsymbol{n}}f\,d\boldsymbol{n} &= \iint\boldsymbol{e}_r\otimes\left(\boldsymbol{e}_\theta\frac{\partial f}{\partial\theta}+\boldsymbol{e}_\varphi\frac{1}{\sin\theta}\frac{\partial f}{\partial\varphi}\right)\sin\theta d\theta d\varphi\\ &= -\iint\left[\frac{\partial}{\partial\theta}(\boldsymbol{e}_r\otimes\boldsymbol{e}_\theta)+\frac{\cos\theta}{\sin\theta}\boldsymbol{e}_r\otimes\boldsymbol{e}_\theta+\frac{1}{\sin\theta}\frac{\partial}{\partial\varphi}(\boldsymbol{e}_r\otimes\boldsymbol{e}_\varphi)\right]f\,\sin\theta d\theta d\varphi\\ &\overset{(B.5)}{=} -\iint\left[\boldsymbol{e}_\theta\otimes\boldsymbol{e}_\theta+\boldsymbol{e}_\varphi\otimes\boldsymbol{e}_\varphi-2\boldsymbol{e}_r\otimes\boldsymbol{e}_r\right]f\,\sin\theta d\theta d\varphi\\ &= \int_{S^2}(3\boldsymbol{n}\otimes\boldsymbol{n}-\mathrm{id})f\,d\boldsymbol{n}\end{aligned}\tag{B.6}$$

Since the final equation in (B.6) is a symmetric tensor, (B.3) follows.

Note that, for any 3×3 matrix κ, the equation holds

$$\nabla_{\boldsymbol{n}}\cdot(P_{\boldsymbol{n}^\perp}\kappa\boldsymbol{n}) = \mathrm{tr}\;\kappa-3\boldsymbol{n}\cdot\kappa\boldsymbol{n}\,,\tag{B.7}$$

where tr stands for the trace operator. Indeed, using (B.5) we obtain

$$\begin{aligned}\nabla_{\boldsymbol{n}}\cdot(P_{\boldsymbol{n}^\perp}\kappa\boldsymbol{n}) &= \left(\boldsymbol{e}_\theta\frac{\partial}{\partial\theta}+\boldsymbol{e}_\varphi\frac{1}{\sin\theta}\frac{\partial}{\partial\varphi}\right)\cdot\left(\kappa\boldsymbol{e}_r-(\boldsymbol{e}_r\cdot\kappa\boldsymbol{e}_r)\boldsymbol{e}_r\right)\\ &\overset{(B.5)}{=} \boldsymbol{e}_\theta\cdot\kappa\boldsymbol{e}_\theta+\boldsymbol{e}_\varphi\cdot\kappa\boldsymbol{e}_\varphi-2\boldsymbol{e}_r\cdot\kappa\boldsymbol{e}_r\\ &= \mathrm{tr}\;\kappa-3\boldsymbol{n}\cdot\kappa\boldsymbol{n}\end{aligned}\tag{B.8}$$

Acknowledgements. This joint research was partially supported by the ACMAC project of the FP7-REGPOt-2009-1 program of the European Commission. FO partially supported by the German Science Foundation through SFB 611. AET partially supported by the National Science Foundation.

REFERENCES

[1] R.B. Bird, Ch.F. Curtiss, R.C. Armstrong, and O. Hassager. *Dynamics of Polymeric Liquids, Vol. 2, Kinetic Theory*. Wiley Interscience, 1987.

[2] J.E. Butler and E.S.G. Shaqfeh. Dynamic simulation of the inhomogeneous sedimentation of rigid fibers. *J. Fluid Mech.*, 468:205–237, 2002.

[3] R.E. Caflish and J.H.C. Luke. Variance in the sedimentation speed of a suspension. *Phys. Fluids*, 28:759–760, 1985.

[4] F.A.C.C. Chalub, P.A. Markowich, B. Perthame, and C. Schmeiser. Kinetic models for chemotaxis and their drift-diffusion limits. *Monatsh. Math.*, 142:123–141, 2004.

[5] M. Doi and S.F. Edwards. *The Theory of Polymer Dynamics*. Oxford University Press, 1986.

[6] J. Dolbeault, P. Markowich, D. Oelz, and C. Schmeiser. Non linear diffusions as limit of kinetic equations with relaxation collision kernels. *Arch. Rational Mech. Anal.*, 186:133–158, 2007.

[7] M. Feist, H. Nirschl, J. Wagner, G. Hirsch, and S. Schabel. Experimental results for the settling behaviour of particle-fiber mixtures. *Physical Separation in Science and Engineering*, 2007.

[8] K. Gustavsson and A.K. Tornberg. Gravity induced sedimentation of slender fibers. *Phys. Fluids*, 21:123301, 2009.
[9] C. Helzel and F. Otto. Multiscale simulations for suspensions of rod-like molecules. *J. Comput. Phys.*, 216(1):52–75, 2006.
[10] B. Herzhaft and É. Guazzelli. Experimental study of the sedimentation of a dilute fiber suspension. *Physical Review Letters*, 77:290–293, 1996.
[11] B. Herzhaft and É. Guazzelli. Experimental study of the sedimentation of dilute and semi-dilute suspensions of fibers. *J. Fluid Mech.*, 384:133–158, 1999.
[12] D.L. Koch and E.S.G. Shaqfeh. The instability of a dispersion of sedimenting spheroids. *J. Fluid Mech.*, 209:521–542, 1989.
[13] J.H.L. Luke. Decay of velocity fluctuations in a stably stratified suspension. *Phys. Fluids*, 12:1619–1621, 2000.
[14] B. Metzger, J.E. Butlerz, and E. Guazzelli. Experimental investigation of the instability of a sedimenting suspension of fibers. *J. Fluid Mech.*, 575:307–332, 2007.
[15] B. Metzger, J.E. Butlerz, and E. Guazzelli. On wavelength selection by stratification in the instability of settling fibers. *Phys. Fluids*, 19:098105, 2007.
[16] F. Otto and A. Tzavaras. Continuity of velocity gradients in suspensions of rod-like molecules. *Comm. Math. Phys.*, 277(3):729–758, 2008.
[17] D. Saintillan, S. Darve, and S.G. Shaqfeh. A smooth particle-mesh ewald algorithm for stokes suspension simulations: The sedimentation of fibers. *Phys. Fluids*, 17:033301, 2005.
[18] D. Saintillan, S.G. Shaqfeh, and E. Darve. The effects of stratification on the wave number selection in the instability of sedimenting spheroids. *Phys. Fluids*, 18:121503, 2006.
[19] D. Saintillan, S.G. Shaqfeh, and E. Darve. The grows of concentration fluctuations in dilute dispersions of orientable and deformable particles under sedimentation. *J. Fluid Mech.*, 553:347–388, 2006.
[20] D. Saintillan and M.J. Shelley. Orientational order and instability in suspensions of self-locomoting rods. *Phys. Rev. Lett.*, 99:058102, 2007.
[21] A.K. Tornberg and K. Gustavsson. A numerical method for simulations of rigid fiber suspensions. *J. Comput. Phys.*, 215:172–196, 2006.
[22] J. Wang and A. Layton. Numerical simulations of fiber sedimentation in Navier-Stokes flows. *J. Comput. Phys.*, 5:61–83, 2009.